Contributions and limitations of environmental magnetism to characterize traffic-related particulate matter sources

Sarah Letaïef, Claire Carvallo, Christine Franke, Aude Isambert, Pierre Camps

Geophysical Journal International

Geophys. J. Int. (2024) **237,** 1505–1525
Advance Access publication 2024 March 18
GJI Geomagnetism and Electromagnetism

https://doi.org/10.1093/gji/ggae108

Contributions and limitations of environmental magnetism to characterize traffic-related particulate matter sources

Sarah Letaïef [1], Claire Carvallo [2], Christine Franke [3], Aude Isambert [4] and Pierre Camps [1]

[1] *Géosciences Montpellier, Université de Montpellier, CNRS, 34095 Montpellier Cedex 05, France*
[2] *Institut de Minéralogie, de Physique des Matériaux et de Cosmochimie, UMR 7590, Sorbonne Université, 75252 Paris Cedex 05, France. E-mail: Claire.Carvallo@impmc.upmc.fr*
[3] *MINES Paris PSL, Center of Geosciences, 77305 Fontainebleau, France*
[4] *Institut de Physique du Globe de Paris, Université Paris Cité, CNRS,* 75005 *Paris, France*

Accepted 2024 March 12. Received 2024 March 11; in original form 2023 September 26

SUMMARY

The chronic exposure to particulate matter (PM) pollution causes societal and environmental issues, in particular in urban areas where most citizen are regularly exposed to vehicular traffic. Since almost two decades, environmental magnetic monitoring has demonstrated its efficiency to successfully map relative concentrations of airborne particle deposition on accumulative surfaces. A better understanding of the magnetic results requires discriminating the main traffic-related sources of the observed signal on particle collectors. To meet this objective, we investigated a sample set of exhaust and non-exhaust sources with respect to their magnetic fingerprints inferred from hysteresis loops, first-order reversal curve (FORC) diagrams, temperature dependency of initial susceptibility and unmixing of isothermal remanent magnetization acquisition curves. The source sample set comprises 14 diesel and gasoline exhaust smoke residues, 12 abrasive-fatigue wear test pieces from worn brake-pads, brake powders, worn tire-tread and three resuspension products: asphalt concrete, street dust and Saharan mineral dust deposited by precipitation after long-range eolian transport. Magnetic properties of the source samples were compared to those from various accumulative surfaces exposed to urban traffic (passive collectors, filters of facemasks for cycling, plant leaves and tree barks). We found some fingerprints of exhaust pipes and brake wear products on these collectors. The findings highlight the relevance of environmental magnetism tools to characterize different traffic-related source signals in accumulative surfaces in urban environment.

Key words: Environmental magnetism; Magnetic mineralogy and petrology; Rock and mineral magnetism.

1. INTRODUCTION

The European Environment Agency reported that in 2019, nearly 307 000 premature deaths were related to chronic exposure to particulate matter (PM) in Europe, besides 40 400 to nitrogen dioxide and 16 800 to ozone exposure (EEA 2021). This makes PM air pollution one of the major environmental, societal and health concerns (Lelieveld *et al.* 2020). Chronic exposure to fine PM (aerodynamic diameter < 2.5 µm $=$ $PM_{2.5}$) is known to be a disease-specific hazard both to the cardiovascular-respiratory system (Konduracka & Rostoff 2022), and to the neurocognitive development (Costa *et al.* 2020). Little is known about the ultrafine PM fraction (aerodynamic diameter < 0.1 µm $=$ $PM_{0.1}$) that is potentially more hazardous. In fact, PM concentrations are measured in $\mu g\,m^{-3}$ by the state-approved air quality measurement agencies following a regulatory directive imposed by the European Union. This directive is objectively ill-suited for monitoring the ultrafine particles in the nanometer size range due to their extremely low mass compared to the fact that they represent by far the most numerous particle population (Seinfeld & Pandis 2016).

The fight to cut down PM pollution is a high priority public health issue, in particular in the context of sustainable urban development. While on 2022 June 8, the European Parliament lawmakers voted to support a proposed ban on the sale of new gas-powered cars by 2035 to diminish greenhouse gas emissions and improve air quality, there is growing evidence that PM emitted through combustion engines is only part of the vehicular origin PM (Charron *et al.* 2019; Grange *et al.* 2021), which might temper the relevance of these policies. Nevertheless, besides the industrial activities and residential heating fired with biomass, road traffic is known to be the main source

of anthropogenic PM exposure in European urban areas (Maher *et al.* 2013; Hama *et al.* 2017). PM emissions originating from vehicle engine fuel combustions and emitted from the tailpipes are called 'exhaust emissions'. 'Non-exhaust emissions' are composed of particles generated from abrasive-fatigue wear processes occurring mainly in the vehicle braking system or in the contact of tires with the road surfaces, and from road dust resuspension produced with the movement of vehicles. Several studies attempted to characterize the elemental composition of the exhaust and non-exhaust emissions. For instance, Fe, Cu, Ba, Sb and Pb are the most important constituents of brake wear (Grigoratos & Martini 2015; Gonet & Maher 2019) and Zn for tire fatigue wear (Thorpe & Harrison 2008; Baensch-Baltruschat *et al.* 2020), while Cr, Zn, S, Cu, Mn, Fe, Ba, Sn, Sb and Br are found in gasoline combustion residues. Ni is present as a product of engine oil combustion, and Br, Ba, Zn, Sb, Cr and Cu are found in diesel combustion residues (Sagnotti *et al.* 2009; Pant & Harrison 2013; Liu *et al.* 2019).

Magnetic measurements of dust deposition samples can provide proxies to map traffic-related pollutants. Most of the Fe-bearing PM released by traffic are ferromagnetic (*sensu lato*) metallic Fe or Fe-oxides, such as magnetite, haematite, or maghaemite (Muxworthy *et al.* 2002; Maher *et al.* 2008; Hansard *et al.* 2012; Sanderson *et al.* 2016). Iron represents the third important traffic emission factor, expressed in μg vehicles^{-1} km^{-1}, after elementary and organic carbon, respectively (Charron *et al.* 2019). Fe-rich particles often absorb trace metals by affinity within their structure, such as C, Ni, Cu, Zn, Ba, Cd, Pb and Mn (Hunt *et al.* 1984; Harrison & Jones 1995; Muxworthy *et al.* 2003; Maher *et al.* 2008; Cao *et al.* 2015; Yang *et al.* 2016). In combustion residues, Fe-bearing nanoparticles can be incorporated into carbon spherules next to various other trace metals (Stone *et al.* 2017). Environmental magnetic methods applied to air quality monitoring are based on a range of concentration, nature, and size dependent parameters to quantify Fe-bearing PM, their associated oxides and trace metals. Originally, these techniques were developed for the study of rocks and soils for (palaeo)environmental applications (e.g. Maher & Thompson 1999). Moreover, studies by Beckwith *et al*. 1986 , Hanesch and Scholger 2002, and Li *et al.* 2001 have shown that Pb, Cu, Zn and ferromagnetic minerals are commonly associated with industrial and traffic-related emissions. In many cities, the measurement of magnetic proxies has proven to be a useful tool to map the relative concentration of PM depositions on accumulative surfaces (e.g. Gautam *et al.* 2005; Hofman *et al.* 2017; Letaïef *et al*. 2023b; Szonyi *et al.* 2008; Sagnotti *et al.* 2009; Winkler *et al.* 2022). While many studies exist based on the identification of anthropogenic PM in soil, the use of various plants (tree leaf and bark), moss or lichen as passive samplers has been popularized because they are omnipresent in cities. They allow sampling at breathing height and provide high-resolution records of spatial and time-integrated information on local air quality (see e.g. Hofman *et al.* 2017, and references therein). Recently, Letaïef *et al.* (2020) have shown that the distribution of particle deposition on accumulating surfaces observed with magnetic measurements was remarkably consistent with that obtained from numerical modelling of the atmospheric dispersion of traffic-related particles. This previous study provides a novel argument reinforcing the relevance of the environmental magnetic approach as a mapping tool for the near-source deposition of particulate pollutants.

Identifying the sources of the acquired magnetic signal is a prerequisite to be able to use this technique in comprehensive source-to-sink surveys (Spassov *et al.* 2004; Sagnotti *et al.* 2006; Winkler *et al.* 2021). The identification of the PM origin solely based on elemental analysis is ambiguous because the same chemical element may stem from different sources. The purpose of this work is to determine distinct magnetic properties by applying a wide variety of techniques commonly employed in rock magnetism laboratories, such as hysteresis measurements, first-order reversal curve (FORC) diagrams, variation of initial susceptibility with temperature and acquisition curves of isothermal remanent magnetization (IRM). To this end, we analysed samples selected from about 30 potential PM sources linked to vehicular traffic in urban areas (exhaust and non-exhaust emissions) checking for specific pattern in each of them. Additionally, we compared the magnetic signal of these potential sources with the magnetic signal of PM deposited on different accumulative surfaces, such as tree leaves, tree barks, as well as passive filters, and pollution mask filters used by cyclists in urban environments.

2. MATERIAL AND METHODS

2.1 Samples

2.1.1 Traffic-related source samples

Exhaust pipe samples were taken either by wiping the inside of the tube end of different vehicle models with a non-magnetic cellulose tissue or by directly removing the powder inside the tailpipe with a plastic spatula (Table 1). We chose cars with various registration dates to study the possible influence of the European emission standards on magnetic characterization (Table SI-1, Supporting Information). We collected between one and four samples from the following types of cars: Euro-1 (1993–1996), Euro-2 (1996–2000), Euro-3 (2001–2003), Euro-4 (2004–2010), Euro-5 (2011–2015) and Euro-6 (past September 2015), including for this latter category one specimen from a hybrid car.

Regarding vehicle wear products (Table 1), we obtained six types of worn brake pads and one worn tire from a car mechanic shop. Although tire wear PM is considered to be responsible for a negligible portion of road dust mainly in the nanometer size (Dahl *et al.* 2006; Foitzik *et al.* 2018), we were interested in characterizing the magnetic properties from this type of source. We sampled worn brake pads and tire tread because the increase in temperature due to heat generation from shear and frictional forces may alter the chemical composition of these materials from their original state. Thus, our samples correspond as close as possible to the car traffic context. The worn brake pads were shredded into millimetre-sized fragments. We removed the surface layer of the tire tread to suppress the material incorporated by the contact of the tire with the road surface. In addition, two samples of brake powder released by abrasive-corrosive wear were collected from the whole braking system of a diesel Euro-4 and a gasoline Euro-3 cars by removing and scraping the dust powder around the wheel rim, the brake disks and pads. Besides, fresh asphalt concrete was recovered on a construction site in the city of Montpellier, France.

Finally, we chose to sample street and mineral dust as wear product of traffic related PM-resuspension. The street dust sample was recovered with a small portable vacuum cleaner in a street in the center of Montpellier where traffic is 7000 veh d^{-1}. *A priori*, we assume that at least all sources of traffic-related PM (exhaust and non-exhaust) may be found in the street dust (Vlasov *et al.* 2022). The mineral dust sample was collected after a Saharan wet-deposition episode in 2020 May, by wiping accumulative surfaces such as car windshields or garden tables with cleaning tissues. Such eolian mineral dust is frequently deposited by precipitation over Europe

Table 1. A comprehensive list of samples used in this study according to their specific methods of sampling and measurement.

Samples	Type	Day Plot	FORC diagrams	k_0 versus temperature	IRM acquisition
Diesel Euro-3	Powder	X	X	X	VSM
Diesel Euro-4.1	Powder	X	X	X	2G-Cryo
Diesel Euro-4.2	Powder	X	X	X	VSM
Gasoline Euro-1	Cellulose tissue	X	X		
Gasoline Euro-2.1	Cellulose tissue	X	X		
Gasoline Euro-2.2	Cellulose tissue	X	X		
Gasoline Euro-3	Cellulose tissue	X	X		
Gasoline Euro-4	Cellulose tissue	X	X		
Gasoline Euro-5	Powder	X	X	X	2G-Cryo
Gasoline Euro-6.1	Cellulose tissue	X	X		
Gasoline Euro-6.2	Cellulose tissue	X	X		
Gasoline Euro-6.3	Cellulose tissue	X	X		
Gasoline Euro-6.4	Cellulose tissue	X	X		
Hybrid Euro-6	Cellulose tissue	X	X		
BrP1	Worn brake pad	X	X	X	VSM
BrP2	Worn brake pad	X	X	X	JR5-A
BrP3	Worn brake pad	X	X	X	VSM
BrP4	Worn brake pad	X	X	X	JR5-A
BrP5	Worn brake pad	X	X	X	VSM
BrP6	Worn brake pad	X	X	X	VSM
Brake dust 1	Powder	X	X	X	JR5-A
Brake dust 2	Powder	X	X	X	VSM
Asphalt	Fresh concrete	X	X	X	2G-Cryo
Tire	Tire thread	X	X		VSM
Mineral dust	Saharan wet-deposition	X	X	X	VSM
Street dust	Canyon street dust	X	X	X	VSM
Bark	*Platanus* bark	X	X		
Plant leaf	*Platanus* leaves	X	X		
Charcoal_Paris	Pollution masks for cyclists	X	X		
Charcoal_Bogotá	Pollution masks for cyclists	X	X		
Electromagnetic_Mexico	Pollution masks for cyclists	X	X		
Electromagnetic_Paris	Pollution masks for cyclists	X	X		
Cercis leaves	Plant leaves	X	X		2G-Cryo
Eleagnus leaves	Plant leaves	X	X		2G-Cryo
Passive filter	Paper filter	X	X		VSM

Notes. For the IRM acquisition experiments, the apparatus used is also specified: 'VSM' is the vibrating sample magnetometer at IPGP; '2G-Cryo' indicated experiments performed at the University of Montpellier using an impulse magnetizer to generate IRMs and a 2G-SQUID or a JR-5 spinner magnetometer.

(Szuszkiewicz *et al.* 2023), and it is a non-negligible but episodic source of PM that can be re-suspended by traffic. However, by sampling a single rain event, this sample is not necessarily representative of all potential dust sources that may have different magnetic signatures (Lyons *et al.* 2012). In the following, we will call this sample mineral dust as it may just as well come from the Sahel zone.

2.1.2 Passive accumulative surface samples

All accumulative surface samples used in this study refer to passive sampling methods. Active sampling from air quality stations, for example, was not considered. We selected tree representative leaf and bark samples that are part of a larger magnetic-monitoring study in the city of Paris (Carvallo *et al*. 2024). Magnetic susceptibility and isothermal remanence magnetic moment of biological samples are usually quite weak, in the order of 10^{-7} m^3 kg^{-1} and 10^{-9} A m^2, respectively. Therefore, we chose samples carrying the strongest magnetic signal to compare them with source signatures. Tree leaf samples from *Platanus* × *acerifolia* and *Populus nigra* were collected in 2012 May at heights around 2 m, at the edge of busy traffic roads riparian to the Seine River and close to major road intersections. The tree bark samples were collected in 2016 February from a plane tree also situated along a busy road along the Seine River, at around ∼1.5 m height.

To enable the most comprehensive comparison with sources, we characterized four pollution masks filters worn by cyclists in Paris, Bogotá, and México City. There are two different types of filters: either electromagnetic (according to the manufacturing company documentation, the filter uses electrostatically charged fibres to attract airborne particulates down to 0.3 μm in size) or active charcoal (95 per cent pure charcoal weave, laminated with medical grade non-woven polypropylene material). The masks were worn for 2–3 weeks (during the year 2019) after which they were visibly dirty. For magnetic measurements, the filters were cut open and the inside layer was tightly packed into gelatin capsules. Therefore, mass normalization was not possible for these samples.

2.2 Measurement methods

2.2.1 Hysteresis properties and FORC diagrams

Measurements of magnetic properties were performed on samples tightly packed in gelatin capsules using a Lakeshore vibrating sample magnetometer (VSM), which is part of the Mineral Magnetism

Analysis Platform at IPGP-IMPMC laboratories. Magnetic hysteresis curves, that is, the variation of the magnetization with an applied field, were measured in maximum applied fields between 0.5 and 1.8 T and enabled us to obtain the values of the major-loop hysteresis parameters, which are the coercive field B_c, the saturation magnetization M_s and the remanent magnetization M_{rs}, respectively. Coercivity of remanence B_{cr} was obtained by backfield curves, which monitor the decrease of the remanent magnetization after saturation with an increasingly negative laboratory field (down to −45 mT). The hysteresis loop parameters were directly corrected for diamagnetic and paramagnetic contributions and are used to calculate the ratios: M_r/M_s and B_{cr}/B_c, are plotted subsequently on a two-variable scatter plot (Day *et al.* 1977). The mixing curves for pure magnetite particles of different domain states (Dunlop 2002) are superimposed on the observed hysteresis data plot to obtain further indications on the domain states of the magnetic carriers present in our samples.

FORC diagrams, calculated from multiple minor hysteresis curves, provide in first approximation information on the distribution of micro coercivities (along the horizontal axis) and interaction fields (along the vertical axis) in a given sample (e.g. Pike *et al.* 1999; Stancu *et al.* 2003; Carvallo *et al.* 2005, 2006). For the weakest magnetized samples, between 10 and 20 individual diagrams were measured and averaged to further decrease the noise on the final FORC diagrams. Averaging times were set at 0.1 or 0.2 s. Magnetic particles with different domain states plot in different areas of the FORC diagram (Roberts *et al.* 2000). Therefore, it is a powerful tool to characterize magnetic domain states for samples containing a mixed domain-size assemblage and/or a range of different coercivities. The resulting diagrams were analysed using the FORCinel software (Harrison & Feinberg 2008), with a variable smoothing factor depending on the type of sample (Egli 2013). Applying larger smoothing factors to the background reduces the noise level considerably while preserving the areas along the axes with relatively small smoothing factors. To compare the diagrams between sources sample, the same smoothing factor was used for all: vertical and central ridge = 10; and horizontal and vertical smoothing = 15.

2.2.2 Scanning electron microscopy

Scanning electron microscopy (SEM) observations were carried out at the IMPMC using a FEG Zeiss Ultra55 SEM. Tree leaves, tree bark and car brake samples were deposited as dry powders in thin layers on carbon tape mounted on SEM stubs. All other samples (Table 1) were left on the cellulose tissue mounted on a stub and observed as is. Stubs were coated with a thin carbon layer (10 nm) to increase electrical conductivity during the observation. Observations were carried out using a backscattered electron (BSE) mode. A Brucker QUANTAX X-ray detector, coupled to the microscope system, was used to perform semi-quantitative elemental analysis through energy dispersive X-ray spectroscopy (EDXS) on individual particles. Data were recorded at 15 kV.

2.2.3 Initial low-field magnetic susceptibility versus temperature

The magnetic susceptibility (k) quantifies the proportion of how magnetizable a material is (Dearing 1999), thus reflecting variations in nature and/or in volumetric concentration of magnetic minerals. Temperature dependence of magnetic susceptibility is typically investigated to determine the Curie temperature of ferromagnetic (*sensu lato*) materials. In this study, we use the normalized initial susceptibility (k_0), which is the initial reversible susceptibility normalized to the k_0 values measured at 20 °C during heating (Dunlop 2014). The temperature dependency of low-field magnetic susceptibility (k_0–T) was investigated using the Agico KLY-3S Kappabridge coupled with a CS-L low-temperature apparatus and a CS-3 furnace temperature control unit at the Geosciences laboratory of the University of Montpellier. The CS-L apparatus has been designed for continuous susceptibility measurements in the range from −194 °C to room temperature. The apparatus is composed of a non-magnetic cryostat with a special platinum thermometer. A small quantity of powder (0.04 to 0.4 g) is put in a silicon glass measuring tube, and then cooled down to −194 °C using liquid nitrogen. Subsequently, the same specimen is placed in the CS-3 non-magnetic furnace to measure a heating-cooling cycle from room temperature up to 700 °C. The raw susceptibility data were corrected for the empty sample holder. Assuming that the Curie temperature(s) detected for a given sample follow a normal distribution, the mean Curie temperature is determined by the inflection point method (Prévot *et al.* 1983), corresponding to the second derivative of the k_0–T curve is zero. The dispersion of the Curie temperature(s) around their mean temperature is characterized by the temperature interval determined by the minimum and the maximum of the second derivative bracketing the mean Curie temperature. Unfortunately, due to the small amount of material in exhaust specimen, only three samples from this category (one diesel Euro-3, one diesel Euro-4, and one gasoline Euro-5) could be used to perform initial magnetic susceptibility versus temperature measurements and unmixing analyses.

2.2.4 IRM acquisition and unmixing analysis

IRM cumulative acquisition is commonly used to identify mixtures of magnetic materials (Robertson & France 1994). Prior to the acquisition, all samples, placed in 8-cc plastic cubes or 0.21-cc transparent gelatin capsules, and their sample holders, were demagnetized applying a 170 mT alternating field. Subsequently, the representative source samples were measured prior to the IRM acquisition to set the baseline. Finally, stepwise IRMs were manually imparted to the sample with an impulse magnetizer, ASC Model IM-10–30, in 30 increments ranging from 1 up to 2800 mT. To prevent any bias due to viscous effects, the samples have been placed in a zero-field for 24 hr right after each IRM acquisition step and prior to measurement. The magnetic moment was measured using a 2G-SQUID magnetometer and an AGICO JR5A spinner magnetometer at the Geosciences laboratory of the University of Montpellier for one sample of diesel, gasoline and asphalt (Table 1), and for strongly magnetized samples such as brake pads, respectively. The measurement steps were chosen to be approximately equidistant on a log-scale. To enrich our data set, we performed additional IRM acquisition curves with the VSM (Table 1). This was possible by first checking on a few samples that the IRM acquisition curves obtained with the VSM are similar to those obtained with the 2 G and the JR5A. For these measurements, the ultrafine/SP fraction of PM is not considered, because IRM acquisition does not consider the magnetic components that are not able to retain a remanent magnetization.

IRM unmixing is an inversion technique used on mixtures of at least two magnetic components to estimate their microcoercivity distributions that fit the bulk sample coercivity distribution contribution given the assumption of a linear additivity. The microcoercivity of a grain depends on several factors, such as the domain size, grain shape, chemical composition, defects and mechanical

stress. By hypothesis, microcoercivity distributions follow a log-normal distribution as long as no magnetic interactions are present (Kruiver *et al.* 2001; Egli 2004). In this case, the progressive IRM acquisition curve acquired by the magnetic assemblages may be approximated by a cumulative log-Gaussian (CLG) function of the magnetizing field (Robertson & France 1994), where each CLG function (or component) is described by three parameters (Robertson & France 1994): (1) the height of the CLG function or its saturation (∼SIRM); (2) the applied field at which half the SIRM is acquired ($B_{1/2}$) and (3) and the dispersion parameter corresponding to the standard deviation of the log-distribution. By deconvoluting the signal, it becomes possible to generate hypotheses concerning the characteristics of the various magnetic carriers and potentially their magnetic behaviour in relation to the size of their magnetic domains. However, it is challenging, if not impossible, to determine the specific concentrations of each component based solely on the height of the CLG functions. This is because the strength of the imparted IRM is heavily influenced by the characteristics of the magnetic materials involved. The inflections observed on the IRM acquisition curve clearly indicate the successive SIRM onsets for each component. Finally, unmixing analysis of the individual log-normal populations that contribute to an IRM bulk distribution were modelled by means of a dedicated computer program created in-house based on a Bayesian approach with a Monte-Carlo-Markov Chains algorithm (Marin & Robert 2014). For further details, the Bayesian method is justified and explained in appendix 2.

3. RESULTS AND DISCUSSION

3.1 Elemental and morphological characterization of PM

Fig. 1 presents representative examples of images obtained by SEM equipped with a BSE detector. The semi-quantitative elemental analyses performed with EDXS corresponding to these images are summarized in Table 2.

3.1.1 SEM of exhaust emission samples

The PM emitted from car exhaust are often constituted of rounded, micro- to nanospheres Fe-bearing particles (Abdul-Razzaq & Gautam 2001; Yang *et al.* 2016) depending on the combustion conditions. However, the images display various particle types, mostly clustered and often irregularly shaped. They are well below the $PM_{2.5}$ size limit in all source samples from vehicles (Fig. 1). The PMs observed in the gasoline Euro-4 exhaust emission sample (Fig. 1a) show both isolated and clustered particles, ranging from 2 to 10 μm. Ten particles were analysed by semi-quantitative elemental analysis. They all show the presence of Fe, and most of them contain a few wt per cent of Ni. Additional metallic elements detected are Cu and Zn in two and three particles, respectively. We identified one particle rich in Cr, and another one rich in Ce, Zr and Pt which may originate from an exhaust gas purifying catalyst (Engler *et al.* 1989). Other elements identified in almost every EDXS analysis are Al, Si, Mg, P, Ca and S.

The SEM images of all gasoline Euro-6 exhaust samples show a mix of isolated particles and clusters (Fig. 1b). Iron is present in all 11 particles studied with EDXS, Cu was detected in 10 particles (0.3–8 wt per cent) and Cr in six particles (0.4–7.2 wt per cent). We also observed Ni in four of them, and up to 3 wt per cent of Zn and Zr in two different particles. Just as in the Euro-4 sample, Mg, Al, Si, P and S are also present, often in small quantities. Individual particles observed on images are frequently smaller than 1 μm.

The presence of Cr, Zn, Cu and Ni in exhaust and exhaust-related emissions is consistent with other studies (e.g. Pant & Harrison 2013). However, because samples were collected by wiping the inside of the exhaust pipe, it cannot be completely excluded that some particles originate from the pipe itself and not from the combustion processes.

3.1.2 SEM of wear product samples

The SEM images from brake powder sample (Fig. 1c) also show numerous individual or clusters of particles with an angular shape, characteristic of particles derived from abrasive wear, and with sizes ranging from 1 to 10 μm. The seven Fe-rich particles analysed with EDXS also show the associated presence of Cu between 0.5 and 2.2 wt per cent, and Al and Si between 0.5 and 5.6 wt per cent. The presence of Cu agrees with results from Pant & Harrison (2013) and Grigoratos & Martini (2015). However, the elemental composition of brake pads can be very diverse. Here, we analysed one type of brake powder, which might probably not be representative of the entire signature of the actual impact of this wear product in the urban PM composition.

3.1.3 SEM of accumulative surface samples

It is very likely that some of the detected elements in the PM are of natural origin, thus not anthropogenic, and represent a detrital mineral background of the urban signal. However, it is difficult to separate the detrital from the anthropogenic signal solely based on their elemental signature. For instance, Si could have a geological origin, as well as industrial or vehicular origin, as it was detected in both exhaust emissions and brake powder.

Selected SEM images of tree leaf and bark samples are presented in Figs 1(d)–(f). Isolated Fe-rich particles ranging from a few micrometres to < 1 μm, are visible on the surface of the plane leaf surface structure (Fig. 1d). Copper is detected in three out of five particles analysed in this sample (2.8–6.7 wt per cent), Zr (2.1 wt per cent), Sb (0.8 wt per cent) and Ba (1.2 wt per cent) in one particle. Plane tree bark samples were investigated as intact bark surface sample (Fig. 1e) and as homogenized dry powder (Fig. 1f). On the intact tree bark surface, we observe the individual particles trapped within the fibre-rich structure of the plane tree bark. Both bark samples show very small particles (< 1 μm) as well as larger particles embedded into the bark fragments. These images demonstrate very well the natural efficiency of tree bark to trap airborne PM. Again, Cu is associated with Fe in these particles (0.6–3.7 wt per cent in 15 out of 22 studied particles) and more occasionally Fe was found next to Ti (0.4–24.6 wt per cent in four particles), Zn (0.5–2.9 wt per cent in three particles), Sn (0.4–2 wt per cent in three particles), Ba (1.4–2.3 wt per cent in two particles) and Cr and Sb (0.8–1.3 wt per cent, respectively, each in one particle). One Zr-rich particle (44 wt per cent) was also identified. Most of the particles analysed on these accumulative surfaces also contain some Al, Si, Mg, Ca and S.

Fig. 1(g) shows a particle cluster deposited on the cyclist mask filter used in Paris, that is composed of one large angular particle (∼10 μm) nested in a cluster of much smaller particles (< 1 μm corresponding to the PM_1 fraction). Fourteen individual particles were analysed with EDXS. They are all Fe-rich, with some contributions of Al, Si and Mg up to a few wt per cent. Cu (2–5 wt per cent) is also present in seven particles, Sn (∼1 wt per cent) was found in four of them, Zn (∼1 wt per cent) in three of them, and Cr and Zr (0.5 wt per cent) in two particles. Finally, the SEM image

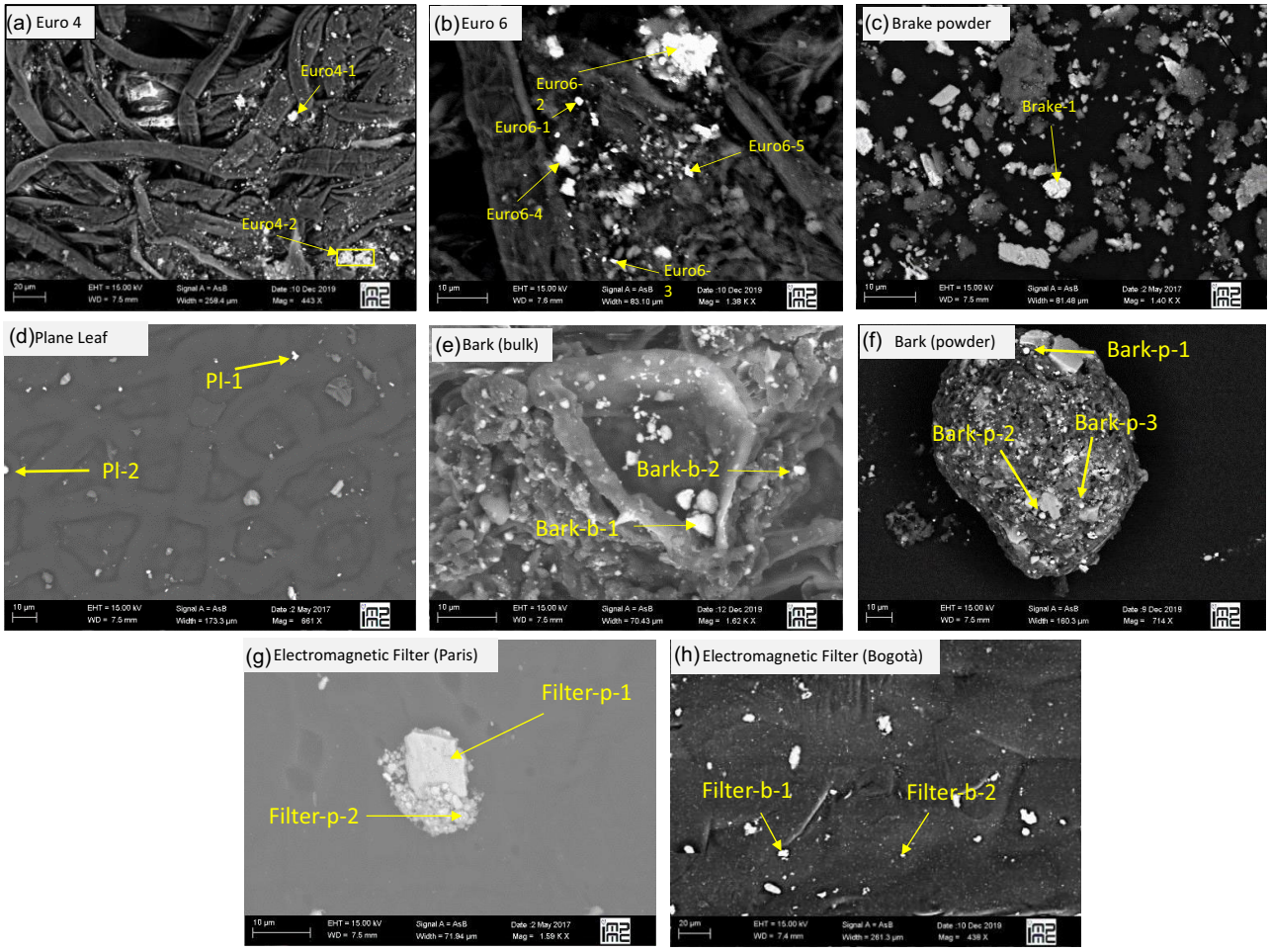

Figure 1. Representative examples of SEM images (using BSE detector) for: (a) gasoline Euro-4 exhaust sample; (b) gasoline Euro-6 exhaust sample; (c) brake powder sample; (d) plane tree leaf sample; (e) and (f) plane tree bark; (g) electromagnetic pollution mask filter from Paris; and (h) electromagnetic pollution mask filter from Bogotá. EDXS spot analysis on PMs is indicated with arrows, results are summarized in Table 2.

of the cyclist mask filter used in Bogotá (Fig. 1h) shows similar particles with sizes from about 20 µm down to the µm ($PM_{2.5}$) and nm ($PM_{0.1}$) size range, with some of them even smaller belonging rather to the $PM_{0.1}$ range. EDXS analyses on 15 PMs show that they are mostly composed of Fe and Si. Calcium, Al, K, Na and Cl are also present (not shown on figures). Unlike the Paris filter, other metallic elements appear only rarely: Zn, Cu and Cr are identified in only one particle.

Almost all accumulative surface samples show the presence of Cu, Zn and Cr, which were also identified in our source samples. Other elements, that were not detected in our source samples are Sn, Ba and Sb. Those elements can nevertheless be found in brake wear as well as exhaust-related products (e.g. Pant & Harrison 2013). However, it seems difficult to discriminate the origin of PM based solely on the elemental composition and PM size, as many elements can be emitted by various sources, and PM sizes are generally very diverse, ranging in all samples from sub-µm to several tens of µm.

3.2 Magnetic domain behaviour

3.2.1 Exhaust emission samples

The Day plot (Fig. 2) allows to separate the samples according to their European norms and their fuel type. The three diesel samples are tightly grouped close to the SD–MD (single domain–multidomain) mixing line, suggesting a contribution equivalent to a mixture of about 70 per cent MD magnetite versus 30 per cent SD magnetite (Dunlop 2002). This result fits well with the specific bimodal particle size distribution for exhaust emissions showing two peaks at 20–40 and 50–90 nm described by Kumar *et al.* (2008) and Liati *et al.* (2012). In contrast, the gasoline samples plot in a large range between the two SD–SP and SD–MD mixing lines, somewhat closer to the MD range. This is different from the results of Sagnotti *et al.* (2009), who found that gasoline samples have a higher contribution of SD magnetite grains than diesel samples, along the mixing line.

As shown by Sheikh *et al.* (2022), the FORC diagrams of the exhaust pipes are described by a signal that extends along the horizontal B_c axis and some vertical spreading around the SP–SD ridge (Fig. 3). Nevertheless, some differences between the Euro norms and the type of fuel may be noted: gasoline Euro-1, Euro-6 and hybrid tailpipe samples are characterized by MD-like behaviours with a wide vertical profile of their FORC distribution and a horizontal profile that does not extend to coercivities higher than 20–25 mT, although this same trend is not notable on the Day plot (Fig. 2). On the contrary, gasoline Euro-2, 3, 4, 5 and diesel Euro-3 as well as 4 tailpipe sample signatures are less extended along the vertical axis and spread along the horizontal axis, to various extents. This could be explained by the contribution of finer SD magnetic particles. However, even if some different patterns may be observed within the same exhaust emission source, the precise distinction between

Table 2. Semi-quantitative EDXS analysis results for the particles indicated with arrows in Fig. 1.

	O	Na	Mg	Al	Si	P	S	Cl	K	Ca	Ti	Cr	Mn	Fe	Ni	Cu	Zn	Zr	Sn	Sb	Ba	Ce	Pt	size (μm)
Euro4-1	24.97			18.49	0.85	2.23	0.46			1.94		2.36		3.26	0.93		0.82	15.32				23.31	5.06	10
Euro4-2	35.43		0.56	3.30	10.11	1.26	0.25		0.43	2.64		3.72		36.66	4.99		0.64							2
Euro6-1	29.32		0.34	0.52	1.58		0.27							65.33		1.23		0.61	0.55					1
Euro6-2	23.30		0.56	7.59	0.38	0.42	2.39	0.45		0.76		1.18		12.59	3.36	8.47								15
Euro6-3	83.39				0.99			1.05		1.40				8.48		3.22								1
Euro6-4	48.05		0.45	0.54	0.47	0.63	0.31							47.30	0.33	1.17								5
Euro6-5	10.05		0.64	0.82	0.61		0.35	0.35				12.44		72.79		1.15								2
Brake-1	8.47			0.45	2.94									86.55		1.59								5
Pl-1	39.67		1.27	1.10	2.42		0.67			0.72				47.23		3.29		2.13		0.71				3
Pl-2	33.84	0.72	0.46	0.78	2.73		0.40	0.14	0.18	0.32			0.47	59.93										5
Bark-b-1	24.22		0.61	0.55	2.30					0.39				71.00		0.61								8
Bark-b-2	16.29			1.03	16.32	0.36	0.71		0.54	3.03				61.54										3
Bark-*p*-1	39.39				0.57									1.25				58.32						3
Bark-*p*-2	8.21		0.38	3.52	24.96		0.27		0.53	18.07	25.32			13.65		0.67								3
Bark-*p*-3	38.05		1.26	1.75	1.46		0.51					1.03		42.10		4.96	3.84		2.86					3
Filter-*p*-1	24.57	0.45	0.39	1.49	1.85		0.58	0.29				0.46	0.43	63.79		3.83		0.54	1.27					15
Filter-*p*-2	21.33	0.94			1.15		0.44	0.76	0.24	0.43				70.82		2.32	0.63				0.24			1
Filter-b-1	45.84	0.62	0.47	11.19	13.98			0.28	2.25	0.57	0.88			23.84										5
Filter-b-2	59.95	0.85	0.40	1.14	0.92			0.22		0.23				35.67										1

Notes. Euro-4: gasoline Euro-4 exhaust sample; Euro-6: gasoline Euro-6 exhaust sample; Brake: brake powder sample; Pl: plane tree leaf sample; Bark-b: bulk plane tree bark; Bark-p: powdered plane tree bark; Filter-p: electromagnetic pollution mask filter from Paris; and Filter-b: electromagnetic pollution mask filter from Bogotá. Because of the presence of Carbon in stubs and coating, C is not included in the EDXS results.

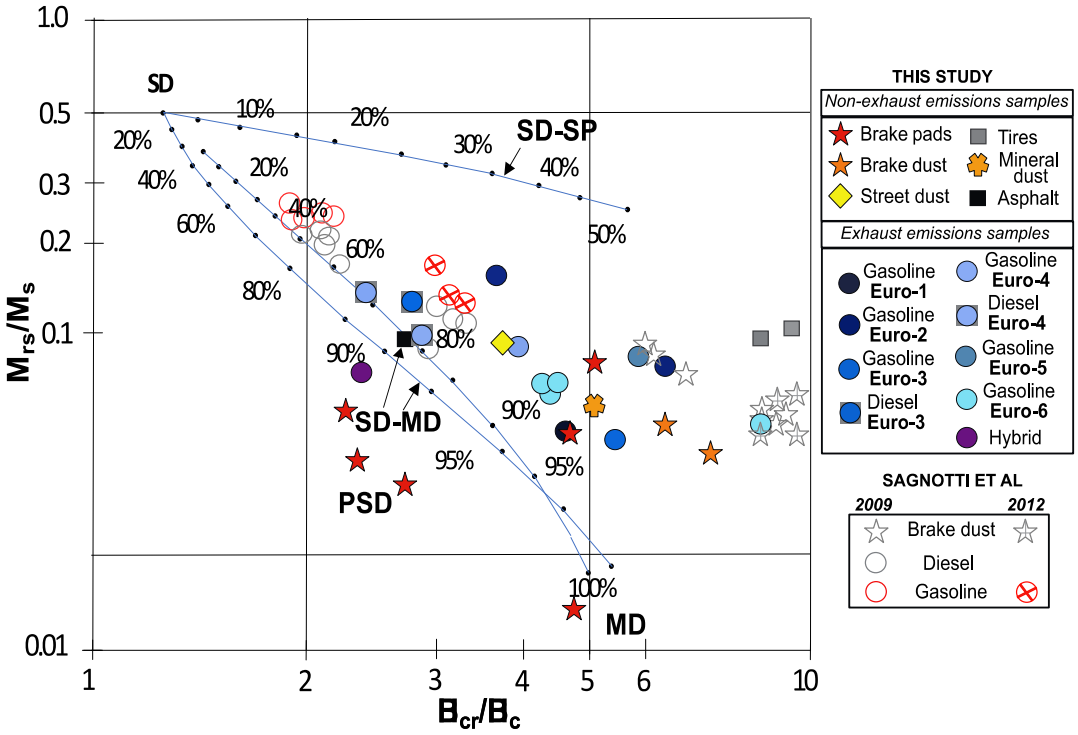

Figure 2. Day plot for: exhaust and non-exhaust emission samples (compared respectively to data from Sagnotti *et al.* 2009; Sagnotti & Winkler 2012). SD: single domain; MD: multidomain; and PSD: pseudo-single domain. Mixing lines for pure magnetite are plotted as continuous lines (Dunlop 2002).

samples exclusively by means of FORCs diagrams remains difficult, as illustrated by the signal heterogeneities between the two gasoline Euro-6 samples.

3.2.2 *Wear product samples*

Hysteresis parameters for brake pads, whether powder or bulk, display a large variability (Fig. 2), suggesting that their composition is heterogeneous. They are mainly characterized by a strong M_s, a small B_c and an M_{rs}/M_s ratio around 0.03. These observations are in line with a previous study that estimated the Fe-content in abrasive wear-derived PM of more than 50 wt per cent (Garg *et al.* 2000), explaining their high contribution to the total measured magnetic signal. In addition, brake pads are known to be a predominant source of non-exhaust PM emissions by contributing to a level of 55.3 per cent ± 7.0 per cent with particle masses in the range of 0.9–11.5 μm aerodynamic diameter (Harrison *et al.* 2012).

Regarding our results on the Day plot (Fig. 2), it appears that the brake pad samples could be segregated into two groups: one defined by a high B_{cr}/B_c ratio (for BrP.3, BrP.4 and BrP.6) and the second by a lower B_{cr}/B_c ratio (for BrP.1, BrP.2 and BrP.5). The latter group is clearly distinguishable from the brake pad powder samples, which plot further on the theoretical trends for SD–MD and SD–SP magnetite grains (Fig. 2). This is consistent with the measurements on brake dust previously reported by Sagnotti *et al.* (2009) and Sagnotti & Winkler (2012). Nevertheless, the hysteresis parameters for two brake pads (BrP.1 and BrP.2) are close to those for the brake powder samples of our study.

In addition, the FORC diagrams for brake pads (Fig. 4) mainly show a mixture of PSD (pseudo-single domain)/MD-like behaviours (Roberts *et al.* 2014) with a large spreading on the B_u axes, except for the BrP.2 sample, which is more PSD-like (Fig. 4c). The difference between brake pads and brake powder from the Day plot is also visible on the FORC diagrams: the brake powder is more PSD-like (Fig. 4a) with a trace of horizontal ridge which could be attributed to an SD contribution with possibly a horizontal ridge visible when smoothing is decreased. This could possibly be attributed to an SP component as shown by Sheikh *et al.* (2022). In any case, the brake powder sample seems to have a lower MD contribution than most brake pads. This could be explained by the fact that the MD particles would be mechanically reduced during abrasion into finer grains with a behaviour that would tend towards that of PSD or SD grains.

Tire samples also plot in between the SD–MD and SP–SD mixing lines on the Day plot, in the region with high B_{cr}/B_c ratios between 6 and 10 (Fig. 2). Only one sample had a magnetization strong enough to perform an FORC diagram (resulting from the average of 12 diagrams). It shows a PSD-like behaviour with a high coercivity tail (Fig. 4h). The asphalt sample plots on the SD–MD theoretical mixing line, suggesting a contribution equivalent to 75 per cent of MD magnetite grains (Fig. 2), but its magnetization was too low to perform any FORC diagram.

3.2.3 *Resuspension product samples*

Road surface wear is responsible for emission of coarser PM (> 10 µm; Kupiainen *et al.* 2005; Gustafsson *et al.* 2008). The mineral and street dust samples plot in the PSD range on the Day plot between the two theoretical line trends (Fig. 2). Both FORC diagrams (Figs 5a and b) show the presence of a range of magnetic domain sizes, from SD to MD, with a contribution of SD magnetite grains that is slightly more important for the urban dust sample than for the mineral dust sample. This is in agreement with Larrasoana *et al.* (2021) and Sagnotti *et al.* (2006), who concluded that the magnetic

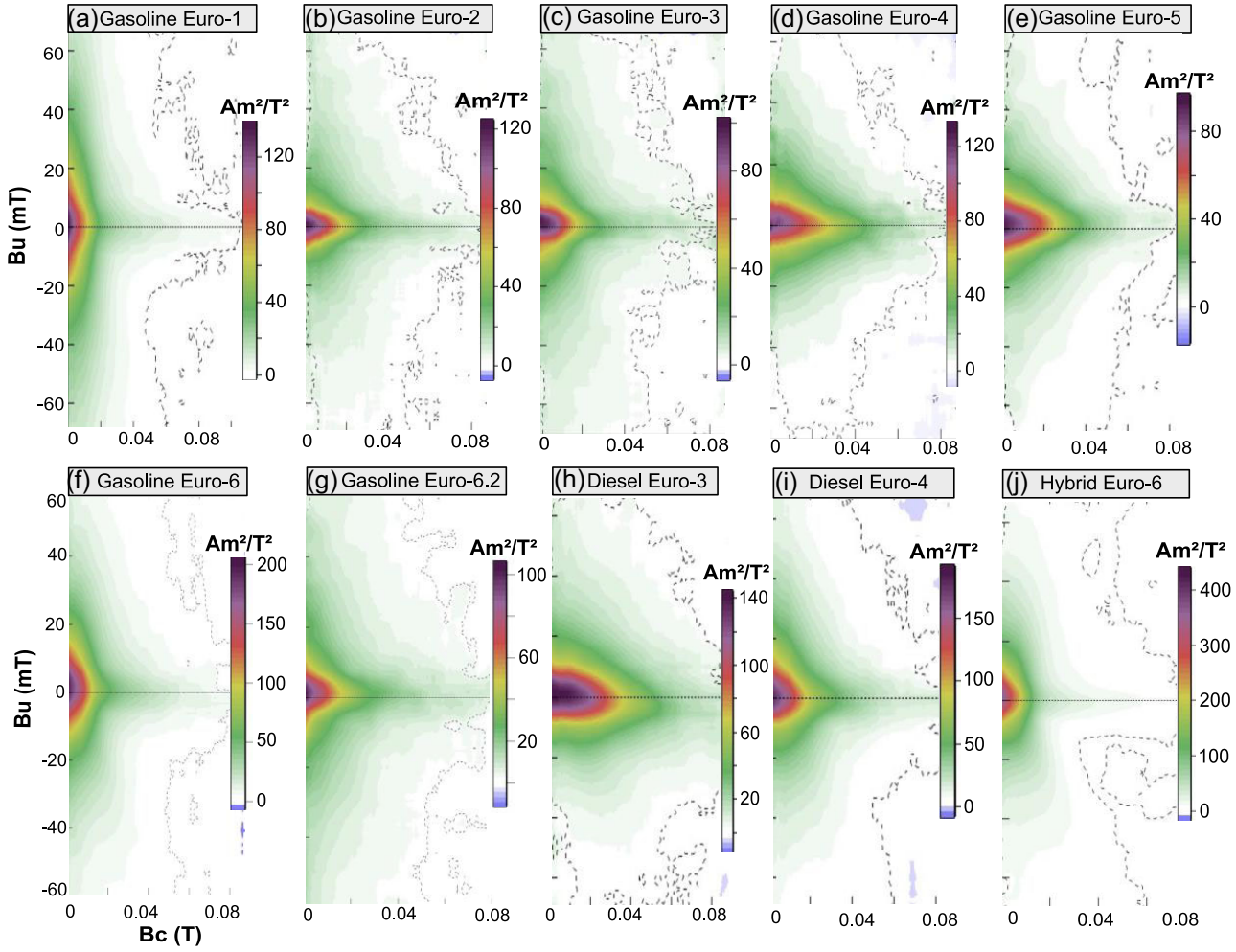

Figure 3. FORC diagrams for the exhaust pipe samples classified according to the fuel type and their respective Euro-norm.

properties of PM10 are not influenced by the presence of high concentration of North African dust, whose magnetic susceptibility is negligible due to the presence of antiferromagnetic minerals. The higher contribution of SD in the street dust sample ties with the observations reported in the literature about the predominance of PM fractions > 1 μm (Muxworthy *et al.* 2002; Kupiainen *et al.* 2005; Duong & Lee 2011; Pant & Harrison 2013) and submicrometric particles (Kupiainen *et al.* 2005).

3.2.4 Accumulative surface samples

All passive samples fall in-between the SD–SP and SD–MD mixing lines (Fig. 6), which is consistent with the results published by Sagnotti *et al.* (2009) and Sagnotti & Winkler (2012).

The two FORC diagrams for plane tree leave and bark (Figs 7a and b) show a similar pattern, which is intermediate between the FORC diagram average pattern of brake pads and those of exhaust pipe samples, as it was also highlighted by Sheikh *et al.* (2022). The general pattern of our passive collector samples agree with those reported by Sagnotti & Winkler (2012) on *Quercus Ilex* leaves in Rome, Italy.

The two active charcoal cyclist filters used in Paris and Bogotá display similar FORC diagrams (Figs 7c and d) with the same amount of spreading along both axes as the FORC diagrams of the biological samples (plant leaves and tree bark). The FORC diagram of the electromagnetic cyclist filter sample from Mexico (Fig. 7e) is different as it extends towards higher coercivities and the spread along the vertical axis is smaller. Finally, the FORC diagram of the electromagnetic cyclist filter from Paris extends slightly less along both axes (Fig. 7f), even if the general aspect is similar to that of the active charcoal filter. We can note that the high coercivity component observed for the filter worn in Mexico, is similar to the component in the Euro-2 to Euro-4 exhaust pipe identified in the FORC diagrams. This could be representative of the generally older vehicles still active in Mexico with less effective filtering engines (International Organization of Motor Vehicle Manufacturers). The average age of the vehicle fleet in France is about 10 yr (European Automobile Manufacturer's Association, Vehicles in use report, 2022), versus ∼16 yr in Mexico (S&P Global Mobility) and ∼17 yr in Colombia (Asociacion Nacional de Movilidad Sostenible). However, it is possible that in the centre of Bogotá, where the respective mask was used, this age is likely to be younger because of the higher living standards in this area. On the opposite, the mask used in Mexico was used in a mixed area combined of countryside and small cities. It must be kept in mind that the climatic and environmental conditions in these three cities are very different, in terms of humidity, wind/air circulation and precipitation rates. The composition

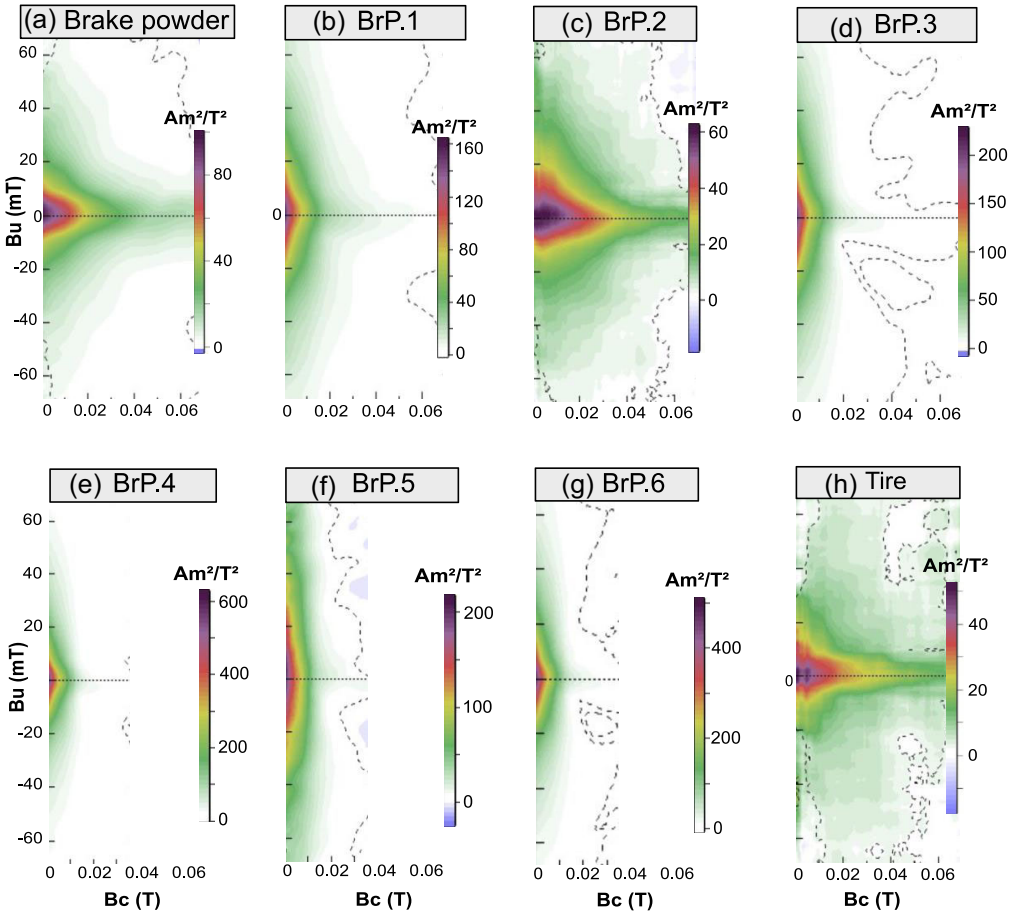

Figure 4. FORC diagrams for vehicle wear products: (a) brake powder and brake pad samples, (b) BrP.1, (c) BrP.2, (d) BrP.3, (e) BrP.4, (f) BrP.5, (g) BrP.6 and (h) tire sample.

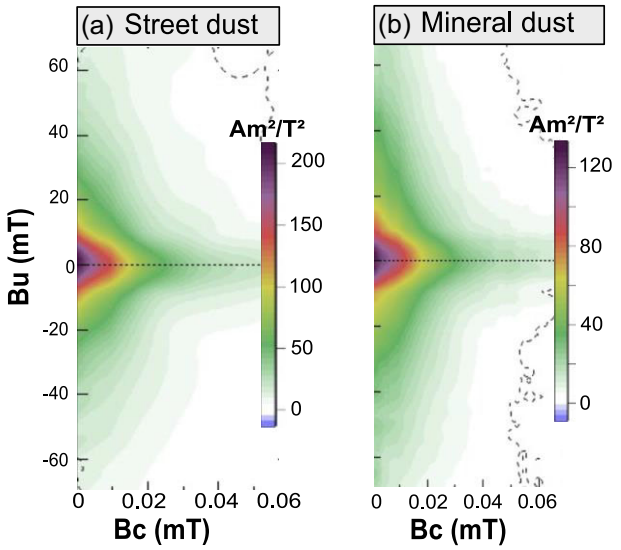

Figure 5. FORC diagrams for resuspension products: (a) street dust, and (b) mineral dust.

of the natural minerals present in soils (lithologic background) deposited on the filters may also have different magnetic compositions and thus varying hysteresis behaviour.

3.3 Magnetic mineralogy

3.3.1 Exhaust emission samples

Because we were unable to perform temperature dependence experiments of initial magnetic susceptibility for the exhaust samples collected with cellulose tissues, we solely compared the thermal behaviour of the diesel Euro-3, diesel Euro-4.1, diesel Euro-4.2 and gasoline Euro-5 samples (Fig. 8). Diesel Euro-3 and diesel Euro-4.2 samples display a very weak signal before reaching the Curie point measured at 588 °C, and a thermochemical transformation that causes the susceptibility to increase by more than one order of magnitude during the cooling, and a change of slope at about 300 °C (Figs 8a and c). This transformation during cooling was also observed for the gasoline Euro-5 sample (Fig. 8d) for which two Curie points were crossed: one at ∼ 500 °C (probably Ti-, Al- and/or Mg-substituted magnetite) and another at 675 °C, suggesting the presence of haematite. However, this transformation is not observed for the diesel Euro-4.1 sample (Fig. 8b), for which the signal seems reversible. To sum up, our results show a wide variety of k_0–T behaviours, therefore, a larger number of such measurements on various exhaust pipe samples (from different Euro-standards and from different types of fuel) would be needed to establish distinct discriminatory criteria based on the variation of susceptibility with temperature.

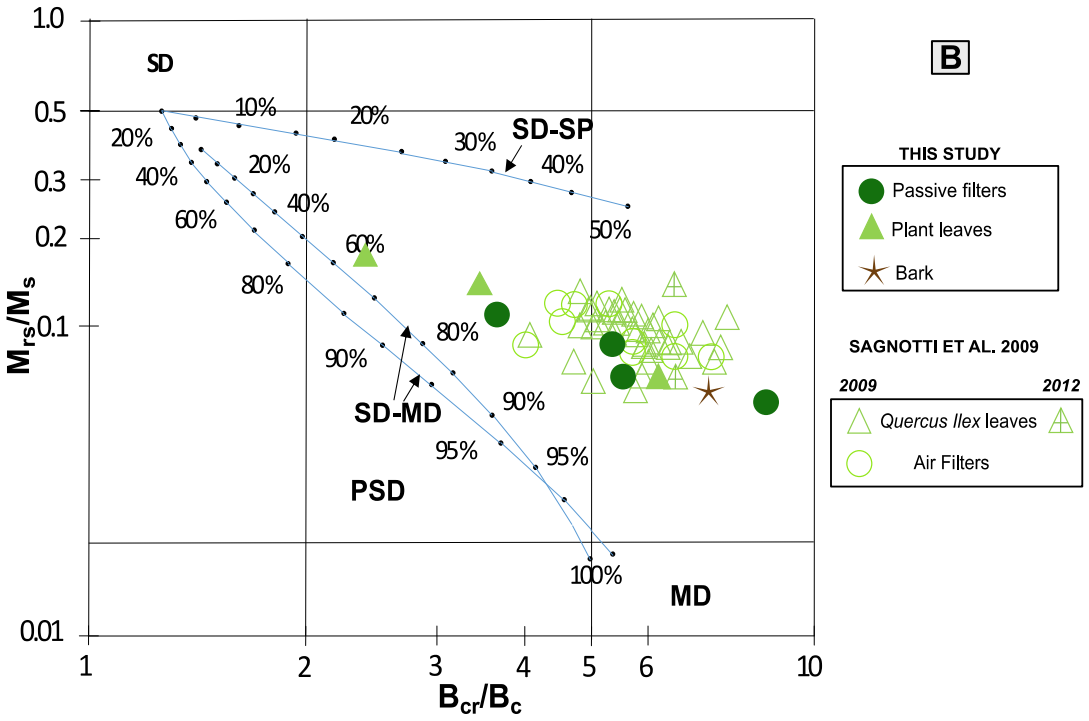

Figure 6. Accumulative surface samples compared to data from Sagnotti *et al.* (2009) and Sagnotti & Winkler (2012). SD: single-domain, MD: multidomain, and PSD: pseudo-single domain. Mixing lines for magnetite are plotted as continuous lines (Dunlop 2002).

The magnetic mineralogy was further investigated with IRM unmixing experiments. The coercivity field distribution signals for the diesel Euro-3 (Fig. 8e), diesel Euro-4.1 (Fig. 8f) and diesel Euro-4.2 (Fig. 8g) exhaust pipe samples are all explained at more than 90 per cent by a main component (C3) centered at 50–60 mT, while another major component at 20 mT is needed to explain the gasoline Euro-5 signal (C2; Fig. 8h). These observations suggest the presence of PSD–MD magnetite-like material as the main magnetization carrier for the diesel samples, as observed on the Day plot, and the additional presence of MD magnetite-like material for the gasoline sample.

Besides, a minor contribution of a higher coercivity component (C4) is observed around 500 mT for all exhaust pipe samples, suggesting the presence of high coercivity material, such as haematite, with a contribution to the total signal of about 4 per cent. Finally, the C1 component located at very low coercivity (< 1 mT) is difficult to interpret, it may explain the slight skewness of the IRM acquisition curve first derivative, which might be caused by magnetic interactions of the C2 component (Egli 2004).

To sum up, the differences between Euro-norms and type fuel, the IRM acquisition signals of these four exhaust pipe samples show two common components: the dominant C3 component between 30 and 60 mT and another high coercivity component C4 at ∼560 mT. These observations are consistent with the k_0–T curves that show a magnetite Curie point after a mineralogy transformation during heating (particularly for diesel Euro-3 and gasoline Euro-5) suggesting the presence of haematite in an oxidizing environment.

3.3.2 *Wear product samples*

The susceptibility temperature dependency curve for the brake powder sample (Fig. 9a) indicates the presence of SD/PSD magnetite-like material as suggested by the large Hopkinson peak at low temperatures and a Curie temperature around 566 °C (Dunlop 2014). In addition, another mineralogical phase characterized by a Curie temperature above 700 °C is present. Regarding the brake pads, we can divide the susceptibility thermomagnetic behaviour into two different groups: one group for samples where magnetite was observed (BrP.1, BrP.2, BrP.5 and BrP.6), and another one for samples where magnetite was not observed (BrP.3 and BrP.4).

Samples BrP.1 (Fig. 9b) and BrP.2 (Fig. 9c) show the presence of the Verwey transition at −152 °C, which is more pronounced for PSD/MD magnetite grains. This suggests the presence of PSD–MD magnetite. In addition, a Curie point close to 560 °C and a flattened Hopkinson peak are observed, indicating the presence of PSD magnetite. Samples BrP.5 (Fig. 9f) and BrP.6 (Fig. 9g) are similar to BrP.2 with a more flattened Hopkinson peak.

Samples BrP.3 (Fig. 9d) and BrP.4 (Fig. 9e) do not display any Verwey transition and the low inflexion at 565 °C suggests a much lower amount of substituted magnetite compared to the other brake pad samples. Nonetheless, a Hopkinson peak is still present as well as a Curie point above 700 °C. The nature of the Hopkinson peak is questionable since it is usually associated with the presence of SD magnetite. However, the Curie temperatures above 700 °C indicate the presence of iron, ferrite, or steel-type materials rather than magnetite (Joshi *et al.* 1988). The Hopkinson peak could be caused by domain wall unpinning in iron (Hopkinson 1889).

The coercivity spectra for the brake samples are different depending on whether the sample is a brake powder (Fig. 9h) or a piece of brake pad (Figs 9i–n), as was also shown in their broad distribution in the Day plot (Fig. 2). The coercivity field distribution for all wear-derived product samples may be explained by the presence of about 80 per cent of a component around 50 mT, which can be related to the presence of PSD–MD magnetite-like material. Note a difference

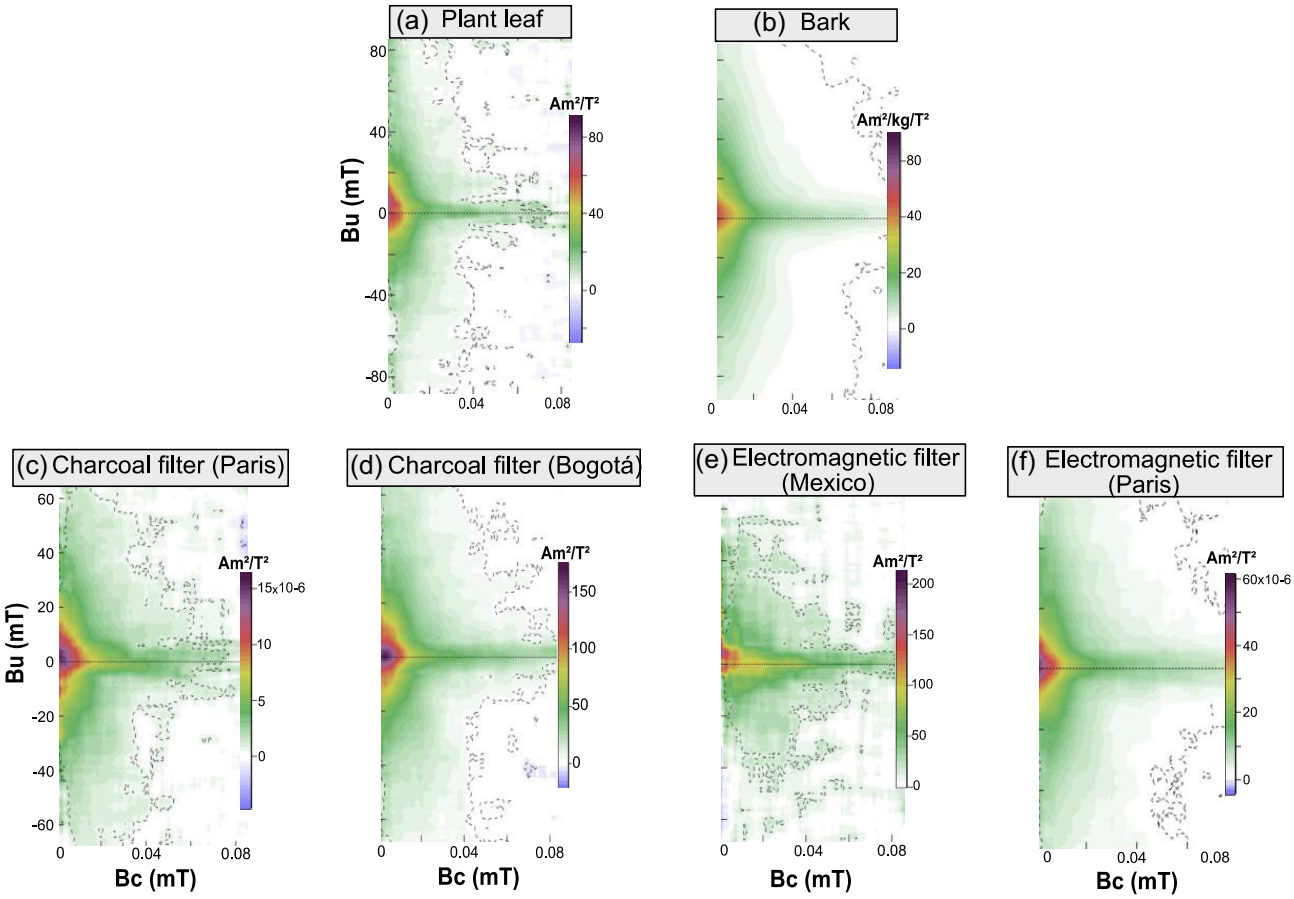

Figure 7. FORC diagrams for (a) plane leaf, (b) plane bark, (c) electromagnetic cyclist filter from Mexico, (d) electromagnetic cyclist filter from Paris, (e) active coal cyclist filter from Paris and (f) active coal cyclist filter from Bogotá.

in trends between brake powder, BrP.1, and BrP.2 on one side and BrP.3, BrP.4, BrP.5 and BrP.6 on the other side. Indeed, the presence of a high coercivity component (C4) around 1 T is found for the latter samples, suggesting the presence of a high coercivity phase with a large proportion, which is not the case for the brake powder, BrP.1, and BrP.2 samples (Figs 9i and j). To summarize, it seems that all brake pads present different magnetic properties, highlighting the variety of compositions and manufacturing techniques from one brand to another. Nevertheless, they all show the presence of iron-steel-like materials, as suggested by Curie temperatures above 700 °C.

The asphalt sample is characterized by a very low initial magnetic susceptibility (Fig. 10a) monitored from room temperature to the sudden increase of susceptibility at 350 °C followed by a rapid decrease around 470 °C. This phenomenon can be attributed to the formation of magnetite during the laboratory heating experiments. Besides, in the cooling curve, a secondary transition around 350 °C suggests the presence of maghaemite-like material probably created by the oxidation of secondary magnetite. This ties in with the presence of three components (Fig. 10b) around 50 mT (C2 and C3) and one other higher than 1 T (C4). Finally, the absence of saturation above 1 T (Fig. 10b) might be associated with a contribution from goethite.

In addition, studies from Milani *et al.* (2004) and Thorpe & Harrison (2008) have shown that tires may be composed of around 50 per cent rubber, 20 per cent of black carbon and 20 per cent of metals including Cu, Cd, and especially Zn. Thus, they are characterized by low concentrations of Fe-bearing nanoparticles, as also highlighted by magnetite hysteresis analyses (Fig. 2). Although we were not able to obtain any k_0–T measurements on tires due to the risk of heating material such rubber samples at high temperatures, we performed IRM acquisition experiments. These analyses allow the identification of three components (Fig. 10c): the first one (C1), with a coercivity around 6 mT is difficult to interpret, whereas the dominant component C2 is located around 50 mT and suggests the contribution of PSD–MD–magnetite-like materials. Finally, the third component at around 600 mT indicates the presence of a mineral with a high coercivity.

3.3.3 *Resuspension product samples*

The resuspension of street dust is a major source of urban PM (Lawrence *et al.* 2013; Pant & Harrison 2013; Vlasov *et al.* 2022) and can be described as a complex mixture of natural soil and traffic-derived PM including both exhaust and non-exhaust emissions (Gonet & Maher 2019). The k_0–T curves for street (Fig. 11a) and mineral dust samples (Fig. 11b) show a high magnetic susceptibility during the heating phase with a Hopkinson effect. In addition, the presence of three successive Curie points at 80, 290 and 567 °C, and probably an unreached one above 700 °C, for the street dust sample. These temperatures suggest the presence of an assemblage

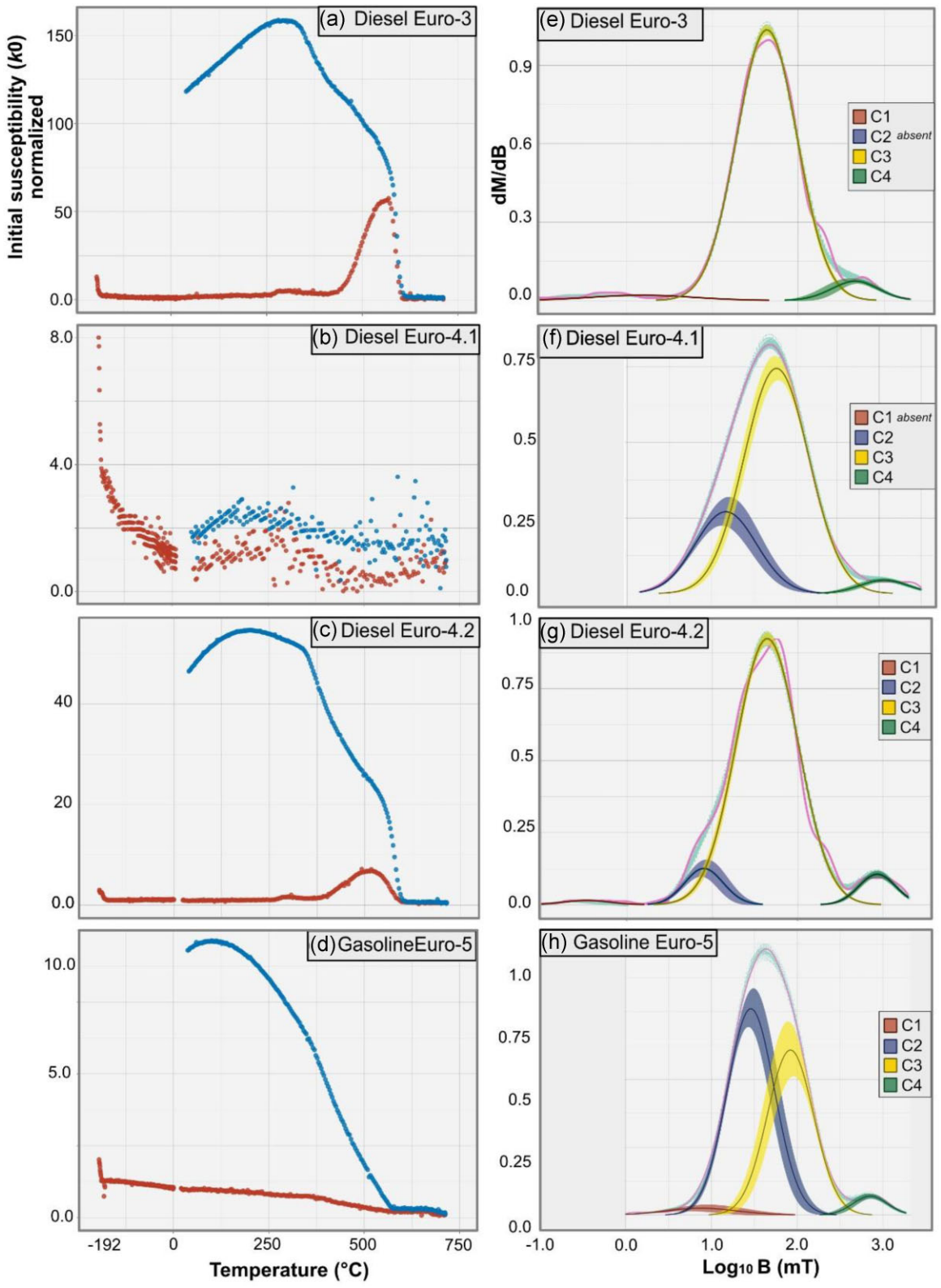

Figure 8. Magnetic mineralogy studied from temperature dependency of magnetic susceptibility (k_0–T curves): (a) diesel Euro-3 exhaust pipe, (b) diesel Euro-4.1, (c) diesel Euro-4.2 and (d) gasoline Euro-5 exhaust pipes. Unmixing of the IRM acquisition curves for: (e) diesel Euro-3, (f) diesel Euro-4.1, (g) diesel Euro-4.2 and (h) gasoline Euro-5; and red line corresponds to heating and blue line to cooling curves.

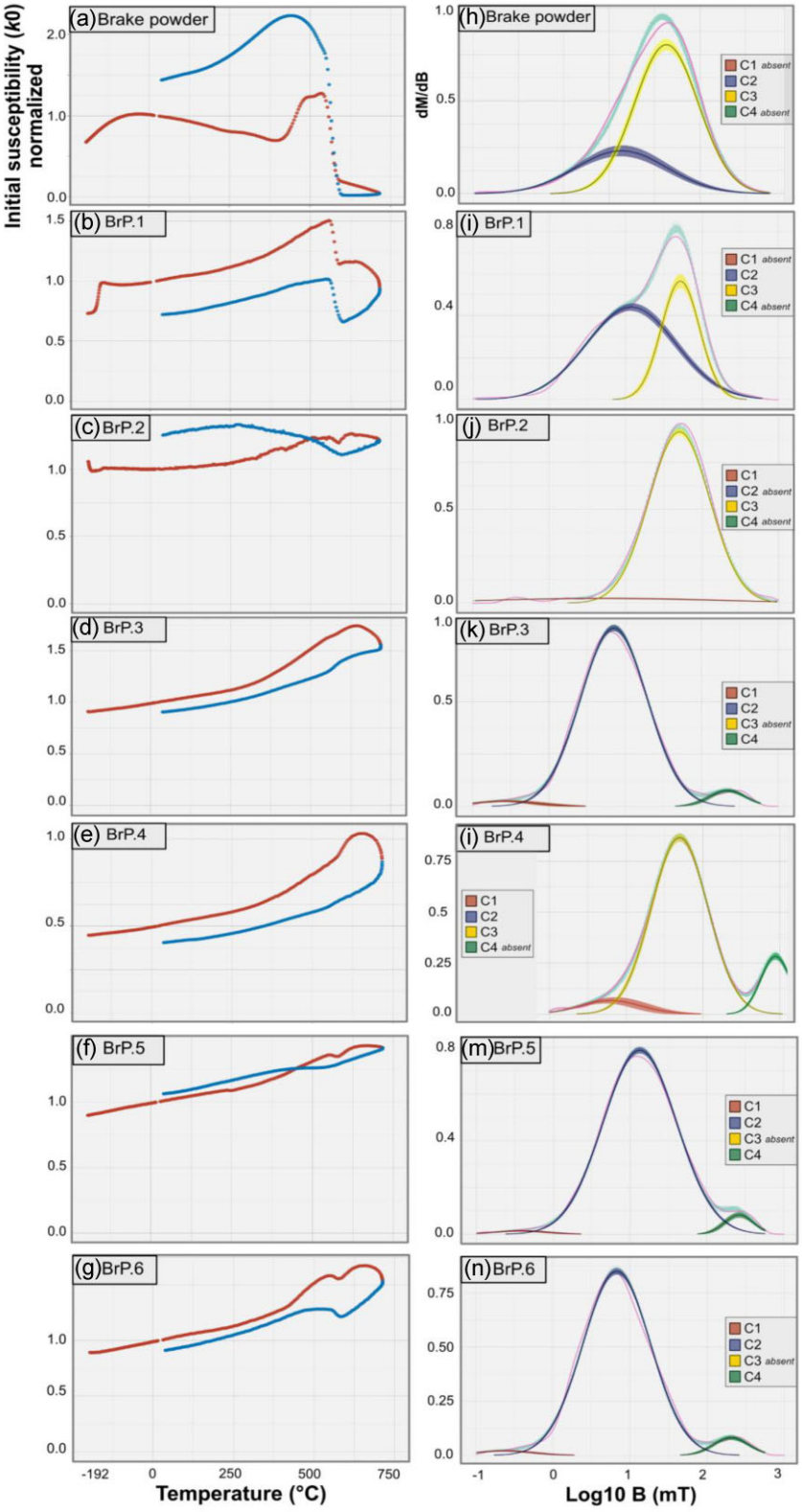

Figure 9. Magnetic mineralogy studied from temperature dependency of magnetic susceptibility (k_0–T curves) and unmixing of the IRM acquisition curve (dM/dB versus $\log_{10}B$) for: (a) and (h) brake powder; (b) and (i) BrP.1, (c) and (j) BrP.2, (d) and (k) BrP.3, (e) and (l) BrP.4, (f) and (m) BrP.5 and (g) and (n) BrP.6.

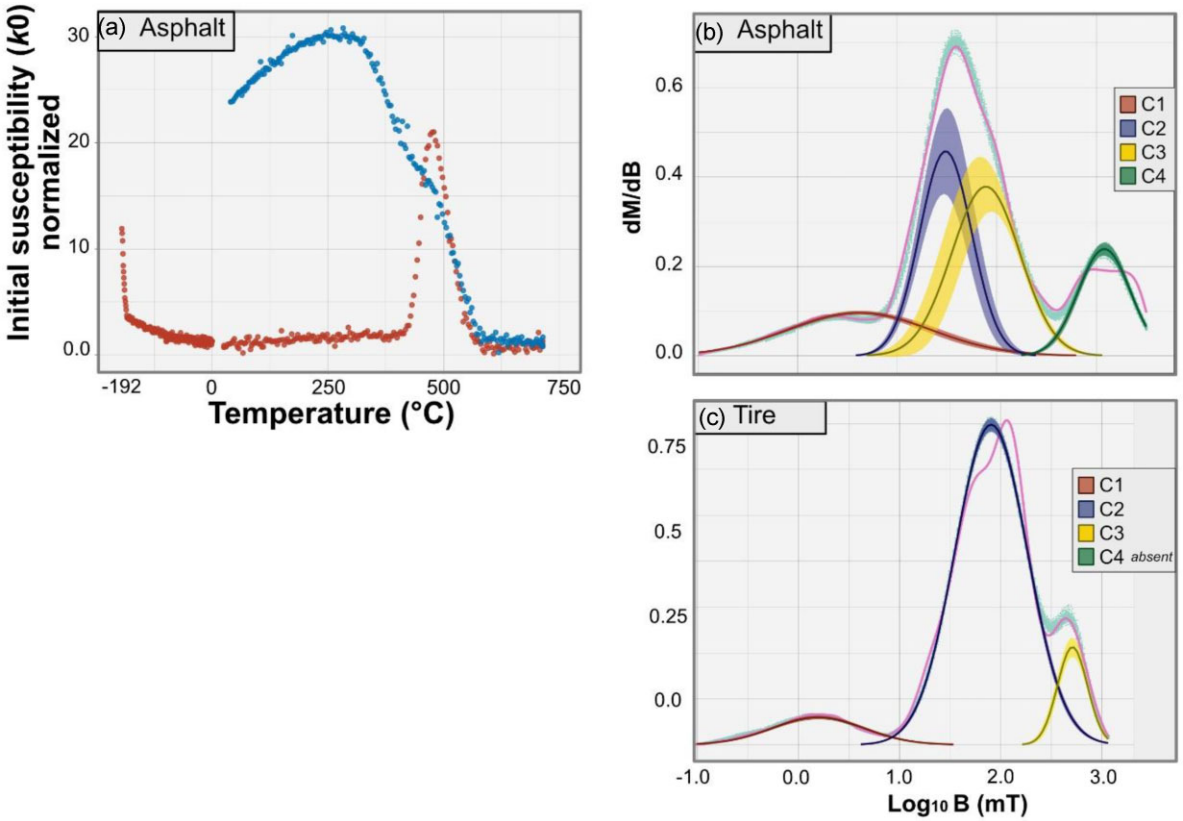

Figure 10. k_0–T curves and IRM unmixing analysis for wear products: (a) and (b) asphalt sample and IRM unmixing analysis for (c) tire 1 sample. For the k_0–T analysis, heating (cooling) curves are represented in red (blue).

of goethite, a non-reversible maghaemite phase, a substituted magnetite supported by a slight Verwey transition at −152 °C, and the presence of iron-cast or steel, respectively. Finally, we also note that the shape of the k_0–T curve of the street dust sample is very similar to that of the brake powder sample, suggesting that brake powder could be an important component of street dust.

The unmixing curve for street dust (Fig. 11c) appears very similar to the one for brake powder (Fig. 9h) with the presence of two low coercivity components (C2 and C3) at around 10 and 30 mT, respectively, suggesting the presence of MD and PSD-like magnetite. These observations tie with several studies, which have shown that roadside submicrometric fractions of PM are characterized by high-Fe concentrations (e.g. Yang *et al.* 2016). This Fe may come in a number of different minerals such as: magnetite, metallic Fe, haematite and other phases (Xie *et al.* 1999, 2001).

Regarding the mineral dust sample (Fig. 11d), we observe a very low coercivity component (C1 < 1 mT), and a mixture of the two components C2 and C3 illustrated in the street dust sample as a C3bis component at 30 mT, suggesting the presence of PSD-like magnetite. Additionally, we note the presence of a third high-coercivity component around 630 mT.

3.3.4 Accumulative surface samples

The passive samples (filters and biological sensors) have a magnetic signal composed of a combination of different potential sources. Indeed, the FORC diagrams of these samples (Fig. 7) display a high coercivity component in the range of 60–80 mT, similar to that obtained from the gasoline Euro-2, 3 and 4 exhaust pipe samples. A strong peak at the origin of the diagram with a vertical spread is also observed and is comparable to what is observed for gasoline Euro-1 and Euro-6 exhaust pipe residuals and brake powder samples. Moreover, the coercivity field distribution from passive samples is explained by three to four magnetic components for plant leave samples (Figs 12a and b), while it was necessary to fit five components for the passive filter (Fig. 12c) sampled in a street canyon. Since the two plant leave samples display a similar distribution shape, while a dis-symmetry of the distribution by two inflexion points are observed for the passive filter sample, which might explain the need for five components instead of four. These slight differences between the samples might be attributed to the nature of the accumulative surfaces themselves.

3.5 Is environmental magnetism methodology efficient to characterize urban air quality?

In many cities, the measurement of magnetic proxies has proven to be an efficient and useful tool to map PM pollution. However, magnetic methods are limited to the detection of magnetic particles. This study is a source-to-sink approach, in which we combine different environmental magnetism techniques to characterize the potential traffic-related sources of PM and evaluate the contribution of each of them to the total magnetic signal measured on accumulative surfaces. The Day plot (Fig. 2) is effective on one hand in discriminating the magnetic signals from sources such as diesel from gasoline exhaust pipes and brakes (whether bulk or powder). On the other hand, the contribution of exhaust pipes and brake powders in the magnetic signal measured on passive sensors, especially plants,

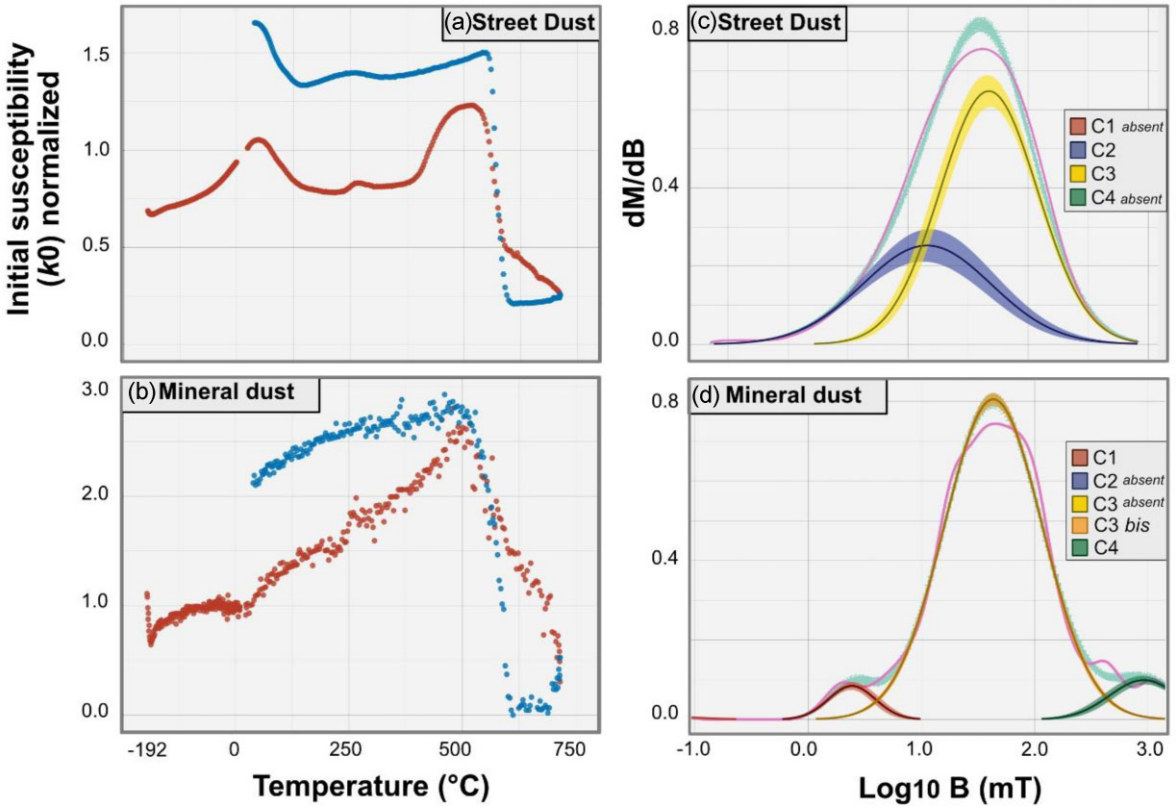

Figure 11. Magnetic mineralogy studied from temperature dependency of magnetic susceptibility (k_0–T curves, left-hand panels) and unmixing of IRM acquisition curves (right-hand panels): (a) and (c) street dust sample; and (b) and (d) mineral dust sample. For the k_0–T analysis, heating (cooling) curves are represented in red (blue).

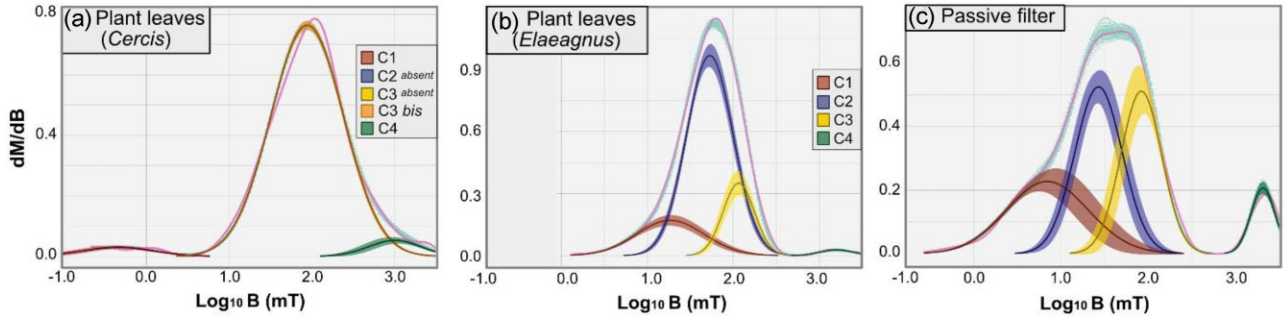

Figure 12. Magnetic mineralogy studied from the unmixing of the IRM acquisition curves for: (a) plant leaves (*Cercis silisquatrum*); (b) plant leaves (*Elaeagnus*) and (c) passive paper filter.

may be determined from a qualitative standpoint since they are found in the same location on the Day plot. Sheikh *et al.* (2022) explained that FORC diagrams show distinctive magnetic fingerprints between the various sources. The authors presented this method as a way to identify and quantify the relative contributions of exhaust and brake pad emissions. The present study, based on a more extended inventory of source categories, complements this previous work and shows a high heterogeneity between samples belonging to the same source type and the difficulty of defining sharp first-order trends. FORC diagrams are not discriminating alone since there are large variations of the magnetic signal measured inside a single source category.

The initial variation in susceptibility with temperature showed that diesel and gasoline exhaust pipes (Figs 8a–c) have very low mass magnetic susceptibility at room temperature (around 10^{-8} $m^3\,kg^{-1}$). This reveals that low-field magnetic susceptibility measured at room temperature is probably not the ideal proxy parameter to determine exhaust emissions contribution in the signal measured on sensors. In addition, it is often not possible to measure the mass of the particles collected on certain sensors due to the very small quantities deposited and the impossibility of extracting them from their support. However, it is a reasonable parameter for discriminating contributions from brake pads from exhaust PM, since our results reveal high magnetic susceptibility values (between 400 and 40 000 10^{-8} $m^3\,kg^{-1}$) at room temperature and the presence of Curie temperatures above 700 °C. Finally, the analysis of the coercivity field distributions derived from IRM acquisition curves provides preliminary results from both different magnetic mineralogy assemblages and grain sizes, as well as their contributions to the total magnetic signal measured.

Table 3. Magnetic parameters characterizing the different sources.

	Day plot and FORC diagrams	Temperature dependency of susceptibility (kT)	Unmixing of IRM acquisition curve
Tailpipes	Diesel : ∼70 per cent MD et 30 per cent SD- magnetite; Gasoline: increase of MD-like behaviour	– Very low susceptibility at room T (°C); – Transformation of magnetic mineral during cooling.	Whether Euro norms, diesel or gasoline: 3 components with a main one (∼30–60 mT) and a high coercivity (∼ 1 T).
Brake pads	Two clusters: (1) 4 mT $< B_{cr} <$ 8 mT—MD-like behaviour; (2) $B_{cr} >$ 14 mT—more PSD-like behaviour	Two clusters: (1) Hopkinson peak—SD/PSD magnetite + magnetite Curie point; + $T_c >$ 700 °C iron/steel; (2) Verwey transition—PSD/MD magnetite + magnetite Curie point, + $T_c >$ 700 °C—iron/steel.	Two clusters: (1) two components: low coercivity-like material; (2) three components including a major one around 50 mT and a high coercivity one around 1T.
Brake powder	Similar to cluster (2) of brake pad: B_{cr} = 30,79 mT—PSD-like behaviour	– Hopkinson peak—SD/PSD magnetite – a slightly lower than magnetite Curie point ∼550 °C	Two components: – C1 ∼ 20 mT—MD-like magnetite, – C2 ∼ 60 mT—PSD-like magnetite.
Street dust	PSD range + slight contribution of SD	– High susceptibility at room temperature; – Hopkinson effect; – Successive Curie points: diverse magnetic mineralogy; – $T_c >$ 700 °C—iron/steel	Two components: – C1 ∼ 10 mT, MD-like magnetite , – C2 ∼ 30 mT, PSD-like magnetite
Mineral dust	PSD range	– High susceptibility at room temperature; – Hopkinson effect	Three components: – C1 < 5 mT, – C3bis (major) ∼ 40 mT—PSD-like magnetite, – C4 around 1T—haematite-like
Tires	– High B_{cr}. – Low M_s and M_r; –PSD-like behaviour FORCs with a high coercivity tail	None	Three components: – C1 = < 1 mT, not interpretable – C2 (major) ∼50 mT—PSD-like magnetite, – C3 ∼500 mT
Asphalt concrete	Contribution of ∼ 75 per cent MD magnetite	– Low susceptibility at room temperature; – Magnetite experimentally found during heating; – Magnetite oxidation during cooling	Four components: - C1 < 1mT—not interpretable; - C2 and C3 ∼50 mT—PSD-like magnetite; – C4 ∼ 1T—haematite-like

The use of accumulative surfaces (passive filters, tree leaves, tree bark, lichens, moss and any other type of accumulative surface) to monitor particle airborne pollution has been popularized because they are low-cost, straight forward to deploy, plants are widely distributed in cities, and these studies could be easily conducted as citizen science studies (Leite *et al.* 2022; Letaïef *et al.* 2023b). These accumulative surfaces allow sampling at breathing height and can provide a high-resolution record of location-specific and time-integrated information on local air quality. For example, Castanheiro *et al.* (2020) measured the magnetic signature and element content of the accumulation of atmospheric dust depositions on leaves in Edegem (Belgium) collected every three weeks throughout a period of three months. Indeed, our results strengthen these conclusions since the magnetic signatures of masks (especially FORC diagrams) are very similar to that of bark and leave samples. Therefore, the use of magnetic properties of biological accumulative surfaces appears to be a realistic proxy to assess the air quality.

Finally, a machine-learning approach such as that proposed by Letaïef *et al.* (2023a), which should be carefully parametrized with the magnetic variables measured in this study may provide a certain ability to predict the main traffic-related source of PM for different kinds of accumulative surfaces. This approach could be an interesting way of tracing traffic-derived pollutants in accumulative surfaces from sources to sinks based on magnetic properties, and to eventually quantify their contributions in the total magnetic signal measured, provided that physical transport processes are well understood and considered in the data acquisition phase and that there are a sufficient quantity of data.

3.6. Proposition for a protocol to identify source signatures on passive accumulative surfaces

Several biases are at play when characterizing the magnetic signature of an accumulative surface. For tree leaves, the rate of deposition depends on the nature and the surface of leaves. The translocation effect could have an impact especially for species intercomparisons. In this way it seems essential to normalize by weight or leaves surface the different magnetic parameters. The roughness of the deposition surface is a key factor in the sensor's ability to retain deposited particles over time (Mitchell *et al.* 2010). Meteorological conditions can also effect on the deposition process (Shu *et al.* 2000; Marié *et al.* 2018). In addition, the distance between the PM

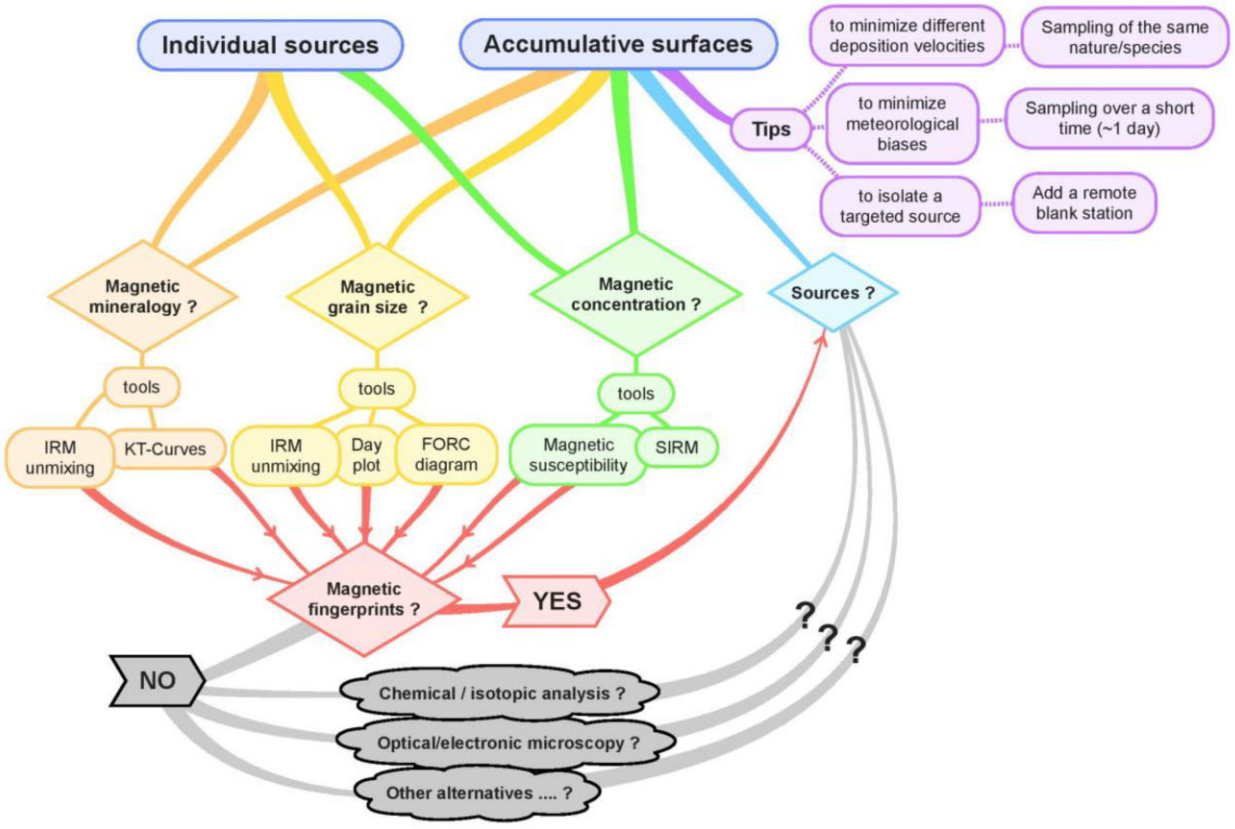

Figure 13. Workflow diagram presenting a suggested general methodology for the use of environmental magnetic proxies collected on accumulative surfaces.

source and the collection surface is a critical parameter (Flanders 1994; Matzka & Maher 1999), not only when measuring extensive parameters such as magnetic susceptibility, but also especially when quantifying the grain size distribution, since finer grains, which are the lightest, travel further than coarser grains. This means that the passive sensors would always have a finer grain size distribution than the sources, directly related to the distance from the source, especially in a multiple PM source environment like the urban one. Nevertheless, based on our measurements (Table 3), we can suggest a first-order protocol for the identification of source signatures in a passive accumulative surface (Fig. 13).

First, we suggest the following three precautions regarding sampling. (i) Sampling should be carried out in a relatively short time window, in order to minimize meteorological bias. (ii) The accumulative surface sampled should be similar, for example, identical species of tree leaves. (iii) In addition, sampling should also be carried out in a background station that does not see the pollution source under study, in order to measure relative variations of a magnetic parameter and to eliminate as many biases as possible (Letaïef *et al.* 2020). One possible way to meet these precautions would be to use lichen transplants, which can be sampled in pristine areas to monitor the magnetic properties change after exposure (Winkler *et al.* 2022).

Three main types of information can be obtained from magnetic measurements. First, magnetic mineralogy can be inferred from IRM unmixing, and k–T curves. The latter are unlikely to be affected by the distance from the source, and the measurements obtained from the sensor are likely to be fairly representative of the source. The grain size distribution, given by hysteresis measurements and IRM unmixing, on the other hand, may be affected by the distance to the source: the information obtained may not be fully representative of the source composition. Finally, measurements of magnetic susceptibility and saturation magnetization, although not carried out in this study, are usually related to the magnetic mineral concentration. It should be noted that remanence measurements do not take into account the SP/ultrafine fraction, which is not able to retain any stable magnetization. Saturation magnetization is the best parameter for evaluating the overall wt per cent concentration of magnetic particles. These measurements may also be subject to biases such as the surface/roughness of the sampled passive accumulator and the distance to the source. Other non-magnetic methods can also give indications on the source identification but these were only marginally touched on in this work.

4. CONCLUSION

A total of 14 tailpipes, six brake-pads, two brake powders, one Sahara mineral dust, one street dust, four tires, one asphalt concrete, three plant leave, one bark and four passive filter samples were analysed using a wide range of environmental magnetism techniques. The study's major results show the strengths and limits of environmental magnetism techniques to characterize various types of traffic-related sources in airborne PM deposited on accumulative surfaces. As these sources are composed of various specimens with heterogeneous magnetic signals, it is difficult to highlight a representative trend for each source and individual magnetic approaches are not necessarily discriminatory. Thus, it is crucial to combine

the different magnetic techniques to outline specific magnetic parameters (summarized in Table 3) and general patterns capable of discriminating source signals. Finally, by comparing the magnetic parameters from accumulative surfaces (passive filters, plant leaves and bark) with those from exhaust and non-exhaust emission sources, it appears that their total magnetic signals are characterized by a combination of source signals (mostly exhaust pipes and brake abrasive-fatigue wear products). A machine-learning approach (e.g. Letaïef *et al.* 2023a) could provide a way to predict the main traffic-related source of PM in accumulative surfaces.

ACKNOWLEDGMENTS

This research was funded by the Agence Nationale de la Recherche (ANR) grant no. ANR-19-CE04-0008. We wish to thank all our colleagues who participated in the sampling of exhaust pipe powder, and Julián Waked for the mask filter from Bogotá. We also thank Imène Estève and Stéphanie Delbrel for their help with SEM measurements. Finally, we thank Karl Fabian and Aldo Winkler for their help in improving the paper, and Eduard Petrovsky for careful editing.

AUTHOR CONTRIBUTIONS

SL: Conceptualization, Methodology, Formal analysis, Data curation, Visualization, Writing—original draft, Writing—review & editing. CC: Conceptualization, Formal analysis, Investigation, Data curation, Writing—original draft, Writing—review & editing. CF: Sampling, Investigation, Writing—review & editing. AI: Sampling Investigation, Writing—review & editing. PC: Conceptualization, Supervision, Resources, Project administration, Funding acquisition, Writing—review & editing.

SUPPORTING INFORMATION

Supplementary data are available at *GJI* online.

Table SI-1. European vehicle standards according to their limit PM concentration (Danielzik 2022, private communication) where the types of fuel have been distinguished: blue for diesels, black for gasolines and orange for hybrids. Note that the car feet proportions are those for France.

Please note: Oxford University Press is not responsible for the content or functionality of any supporting materials supplied by the authors. Any queries (other than missing material) should be directed to the corresponding author for the paper.

DECLARATION OF COMPETING INTEREST

The authors declare that they have no known competing financial interests or personal relationships that could have appeared to influence the work reported in this paper.

DATA AVAILABILITY

Data are available in Zenodo repository: https://doi.org/10.5281/zenodo.8359488

REFERENCES

Abdul-Razzaq, W. & Gautam, M., 2001. Discovery of magnetite in the exhausted material from a diesel engine. *Appl. Phys. Lett.,* **78,** 2018–2019.

Baensch-Baltruschat, B., Kocher, B., Stock, F. & Reifferscheid, G., 2020. Tyre and road wear particles (TRWP)—a review of generation, properties, emissions, human health risk, ecotoxicity, and fate in the environment. *Sci. Total Environ.,* **733,**

Beckwith, P.R., Ellis, J.B. & Revitt, D.M., 1986, Heavy metal and magnetic relationships for urban source sediments. *Phys Earth Planet Int,* **42,** 67–75.

Cao, L., Appel, E., Rosler, W. & Magiera, T., 2015. Efficiency of stpwise magnetic-chemical site assessment for fly-ash derived heavy metal pollution. *Geophys. J. Int.,* **203**(2), 767–775.

Carvallo, C., Dunlop, D.J. & Özdemir, Ö., 2005. Experimental comparison of FORC and remanent Preisach diagrams. *Geophys. J. Int.,* **162,** 747–754.

Carvallo, C. *et al.*, ., 2024. EcorçAir : a citizen science project for the biomonitoring of vehicular air pollution in Paris, France. *Submitted to Community Science*

Carvallo, C., Roberts, A.P., Leonhardt, R., Laj, C., Kissel, C., Perrin, M. & Camps, P., 2006. Increasing the efficiency of paleointensity analyses by selection of samples using first-order reversal curve diagrams. *J. geophys. Res. Solid Earth,* **111**.

Castanheiro, A. *et al.* 2020. Leaf accumulation of atmospheric dust: biomagnetic, morphological and elemental evaluation using SEM, ED-XRF and HR-ICP-MS. *Atmos. Environ.,* **221,** 117082.

Charron, A. *et al.* 2019. Identification and quantification of particulate tracers of exhaust and non-exhaust vehicle emissions. *Atmos. Chem. Phys.,* **19,** 5187–5207.

Costa, L.G., Cole, T.B., Dao, K., Chang, Y.-C., Coburn, J. & Garrick, J.M., 2020. Effects of air pollution on the nervous system and its possible role in neurodevelopmental and neurodegenerative disorders. *Pharmacol. Ther.,* **210,**

Dahl, A., Gharibi, A., Swietlicki, E., Gudmundsson, A., Bohgard, M., Ljungman, A., Blomqvist, G. & Gustafsson, M., 2006. Traffic-generated emissions of ultrafine particles from pavement–tire interface. *Atmos. Environ.,* **40,** 1314–1323.

Day, R., Fuller, M. & Schmidt, V.A., 1977. Hysteresis properties of titanomagnetites: grain-size and compositional dependence. *Phys. Earth Planet. Inter.,* **13,** 260–267.

Dearing, J., 1999. Environmental Magnetic susceptibility—using the Bartington MS2 system. Chi Publishing, England, 54 pp.

Dunlop, D.J., 2002. Theory and application of the day plot (M rs /M s versus H cr / H c) 2. Application to data for rocks, sediments, and soils. *J. geophys. Res.,* **107,** 10.1029/2001JB000486.

Dunlop, D.J., 2014. High-temperature susceptibility of magnetite: a new pseudo-single-domain effect. *Geophys. J. Int.,* **199,** 707–716.

Duong, T.T.T. & Lee, B.-K., 2011. Determining contamination level of heavy metals in road dust from busy traffic areas with different characteristics. *J. Environ. Manage.,* **92,** 554–562.

EEA, 2021. Air quality in Europe 2021. Copenhagen. doi:10.2800/549289.

Egli, R., 2004. Characterization of individual rock magnetic components by analysis of remanence curves, 1. Unmixing natural sediments. *Stud. Geophys. Geod.,* **48,** 391–446.

Egli, R., 2013. VARIFORC: an optimized protocol for calculating non-regular first-order reversal curve (FORC) diagrams. *Glob. Planet. Change,* **110,** 302–320.

Engler, B., Koberstein, E. & Schubert, P., 1989. Automotive exhaust gas catalysts: surface structure and activity. *Appl. Catal.,* **48,** 71–92.

Flanders, P.J., 1994. Collection, measurements and analysis of airborne magnetic particulates from pollution in the environment. *J. appl. Phys.,* **75,** 5931–5936.

Foitzik, M.-J., Unrau, H.-J., Gauterin, F., Dörnhöfer, J. & Koch, T., 2018. Investigation of ultra fine particulate matter emission of rubber tires. *Wear,* **394–395,** 87–95.

Garg, B.D., Cadle, S.H., Mulawa, P.A., Groblicki, P.J., Laroo, C. & Parr, G.A., 2000. Brake wear particulate matter emissions. *Environ. Sci. Technol.,* **34,** 4463–4469.

Gautam, P., Blaha, U. & Appel, E. 2005. Magnetic susceptibility of dust-loaded leaves as a proxy of traffic-related heavy metal pollution in Kathmandu city. *Nepal. Atmos. Environ.,* **39,** 2201–2211.

Gonet, T. & Maher, B.A., 2019. Airborne, vehicle-derived Fe-bearing nanoparticles in the urban environment: a review. *Environ. Sci. Technol.,* **53,** 9970–9991.

Grange, S.K. *et al.* 2021. Switzerland's PM10 and PM2.5 environmental increments show the importance of non-exhaust emissions. *Atmos. Environ. X,* **12,** doi:10.1016/j.aeaoa.2021.100145.

Grigoratos, T. & Martini, G., 2015. Brake wear particle emissions: a review. *Environ. Sci. Pollut. Res.,* **22,** 2491–2504.

Gustafsson, M., Blomqvist, G., Gudmundsson, A., Dahl, A., Swietlicki, E., Bohgard, M., Lindbom, J. & Ljungman, A., 2008. Properties and toxicological effects of particles from the interaction between tyres, road pavement and winter traction material. *Sci. Total Environ.,* **393,** 226–240.

Hama, S.M.L., Cordell, R.L. & Monks, P.S., 2017. Quantifying primary and secondary source contributions to ultrafine particles in the UK urban background. *Atmos. Environ.,* **166,** 62–78.

Hanesch, M. & Scholger, R., 2002, Mapping of heavy metal loadings in soils by means of magnetic susceptibility measurements. *Environ. Geol.,* **42,** 857–870, doi:10.1007/s00254-002-0604-1.

Hansard, R., Maher, B.A. & Kinnersley, R.P., 2012. Rapid magnetic biomonitoring and differentiation of atmospheric particulate pollutants at the roadside and around two major industrial sites in the U.K. *Environ. Sci. Technol.,* **46,** 4403–4410.

Harrison, R.J. & Feinberg, J.M., 2008. FORCinel: an improved algorithm for calculating first-order reversal curve distributions using locally weighted regression smoothing. *Geochem. Geophys. Geosyst.,* **9,** doi:10.1029/2008GC001987.

Harrison, R.M. & Jones, M., 1995. The chemical composition of airborne particles in the UK atmosphere. *Sci. Total Environ.,* **168,** 195–214.

Harrison, R.M., Jones, A.M., Gietl, J., Yin, J. & Green, D.C., 2012. Estimation of the contributions of brake dust, tire wear, and resuspension to nonexhaust traffic particles derived from atmospheric measurements. *Environ. Sci. Technol.,* **46,** 6523–6529.

Hofman, J., Maher, B.A., Muxworthy, A.R., Wuyts, K., Castanheiro, A. & Samson, R., 2017. Biomagnetic monitoring of atmospheric pollution: a review of magnetic signatures from biological sensors. *Environ. Sci. Technol.,* **51,** 6648–6664.

Hopkinson, J., 1889. Magnetic and other physical properties of iron at a high temperature. *Phil. Trans. R. Soc. Lond,* **180A,** 443–465

Hunt, A., Jones, J. & Oldfield, F., 1984. Magnetic measurements and heavy metals in atmospheric particulates of anthropogenic origin. *Sci. Total Environ.,* **33,** 129–139.

Joshi, G.K., Khot, A.Y. & Sawant, S.R., 1988. Magnetisation, curie temperature and Y□K angle studies of Cu substituted and non substituted Ni□Zn mixed ferrites. *Solid State Commun.,* **65,** 1593–1595.

Konduracka, E. & Rostoff, P., 2022. Links between chronic exposure to outdoor air pollution and cardiovascular diseases: a review. *Environ. Chem. Lett.,* **20,** 2971–2988,

Kruiver, P.P., Dekkers, M.J. & Heslop, D., 2001. Quantification of magnetic coercivity components by the analysis of acquisition curves of isothermal remanent magnetisation. *Earth planet. Sci. Lett.,* **189,** 269–276.

Kumar, P., Fennell, P., Langley, D. & Britter, R., 2008. Pseudo-simultaneous measurements for the vertical variation of coarse, fine and ultrafine particles in an urban street canyon. *Atmos. Environ.,* **42,** 4304–4319.

Kupiainen, K.J., Tervahattu, H., Räisänen, M., Mäkelä, T., Aurela, M. & Hillamo, R., 2005. Size and composition of airborne particles from pavement wear, tires, and traction sanding. *Environ. Sci. Technol.,* **39,** 699–706.

Larrasoana, J.C. *et al.*, 2021. Environmental magnetic fingerprinting of anthropogenic and natural atmospheric deposition over southwestern Europe. *Atmos. Environ.,* **261,** doi:10.1016/j.atmosenv.2021.118568.

Lawrence, S., Sokhi, R., Ravindra, K., Mao, H., Prain, H.D. & Bull, I.D., 2013. Source apportionment of traffic emissions of particulate matter using tunnel measurements. *Atmos. Environ.,* **77,** 548–557.

Leite, A.d.S. *et al.*, 2022. Barking up the right tree: using tree bark to track airborne particles in school environment and link science to society. *GeoHealth,* **6,** doi:10.1029/2022GH000633.

Lelieveld, J., Pozzer, A., Pöschl, U., Fnais, M., Haines, A. & Münzel, T., 2020. Loss of life expectancy from air pollution compared to other risk factors: a worldwide perspective. *Cardiovasc. Res.,* **116,** 1910–1917.

Letaïef, S., Camps, P. & Carvallo, C., 2023a. A supervised machine learning approach to classify traffic-derived PM sources based on their magnetic properties. *Environ. Res.,* **231,** doi:10.1016/j.envres.2023.116006.

Letaïef, S., Camps, P., Poidras, T., Nicol, P., Bosch, D. & Pradeau, R., 2020. Biomagnetic monitoring vs. CFD modeling: a real case study of near-source depositions of traffic-related particulate matter along a motorway. *Atmosphere,* **11,** doi:10.3390/atmos11121285.

Letaïef, S., Scotto-d'Apollonia, L., Dosias-Perla, D., Pinero, C., Perier, R., Nicol, P. & Camps, P., 2023b. Benefits and limitations of environmental magnetism for completing citizen science on air quality: a case study in a street canyon. *Community Sci,* **2**. doi:10.1029/2022CSJ000010.

Li, X.D., Poon, C.S. & Liu, P.S., 2001. Heavy metal contamination of urban soils and street dusts in Hong Kong. *Appl. Geochem.* **16,** 1361–1368

Liati, A., Spiteri, A., Dimopoulos Eggenschwiler, P. & Vogel-Schäuble, N., 2012. Microscopic investigation of soot and ash particulate matter derived from biofuel and diesel: implications for the reactivity of soot. *J. Nanoparticle Res.,* **14,** doi:10.1007/s11051-012-1224-7.

Liu, H., Yan, Y., Chang, H., Chen, H., Liang, L., Liu, X., Qiang, X. & Sun, Y., 2019. Magnetic signatures of natural and anthropogenic sources of urban dust aerosol. *Atmos. Chem. Phys.,* **19,** 731–745.

Lyons, R., Oldfield, F. & Williams, E., 2012. The possible role of magnetic measurements in the discrimination of Sahara/Sahel dust sources. *Earth Surf. Process. Landforms,* **37,** 594–606.

Maher, B. & Thompson, R., 1999. *Quaternary Climates, Environments and Magnetism, Quaternary Climates, Environments and Magnetism*. Cambridge University Press.

Maher, B.A., Ahmed, I.A.M., Davison, B., Karloukovski, V. & Clarke, R., 2013. Impact of roadside tree lines on indoor concentrations of traffic-derived particulate matter. *Environ. Sci. Technol.,* **47,** 13737–13744.

Maher, B.A., Moore, C. & Matzka, J., 2008. Spatial variation in vehicle-derived metal pollution identified by magnetic and elemental analysis of roadside tree leaves. *Atmos. Environ.,* **42,** 364–373.

Marié, D.C., Chaparro, M.A.E., Lavornia, J.M., Sinito, A.M., Castañeda Miranda, A.G., Gargiulo, J.D., Chaparro, M.A.E. & Böhnel, H.N., 2018. Atmospheric pollution assessed by in situ measurement of magnetic susceptibility on lichens. *Ecol. Indic.,* **95**(1), 831–840.

Marin, J.-M. & Robert, C.P., 2014. Mixture Models. in: *Bayesian Essentials with R, Springer Texts in Statistics*. Springer New York, NY, pp. 173–207.

Matzka, J. & Maher, B.A., 1999. Magnetic biomonitoring of roadside tree leaves: identification of spatial and temporal variations in vehicle-derived particulates. *Atmos. Environ.,* **33,** 4565–4569.

Milani, M., Pucillo, F.P., Ballerini, M., Camatini, M., Gualtieri, M. & Martino, S., 2004. First evidence of tyre debris characterization at the nanoscale by focused ion beam. *Mater. Charact.,* **52,** 283–288.

Mitchell, R., Maher, B.A. & Kinnersley, R., 2010. Rates of particulate pollution deposition onto leaf surfaces: temporal and inter-species magnetic analyses. *Environ Poll,* **158,** 1472–1478

Muxworthy, A.R., Matzka, J., Davila, A.F. & Petersen, N., 2003. Magnetic signature of daily sampled urban atmospheric particles. *Atmos. Environ.,* **37,** 4163–4169.

Muxworthy, A.R., Schmidbauer, E. & Petersen, N., 2002. Magnetic properties and Mössbauer spectra of urban atmospheric particulate matter: a case study from Munich, Germany. *Geophys. J. Int.,* **150,** 558–570.

Pant, P. & Harrison, R.M., 2013. Estimation of the contribution of road traffic emissions to particulate matter concentrations from field measurements: a review. *Atmos. Environ.,* **77,** 78–97.

Pike, C.R., Roberts, A.P. & Verosub, K.L., 1999. Characterizing interactions in fine magnetic particle systems using first order reversal curves. *J. appl. Phys.,* **85,** 6660–6667.

Prévot, M., Mankinen, E.A., Grommé, S. & Lecaille, A., 1983. High paleointensities of the geomagnetic field from thermomagnetic studies on

Rift Valley pillow basalts from the Mid-Atlantic Ridge. *J. geophys. Res.,* **88,** 2316–2326. doi:10.1029/JB088iB03p02316.

Roberts, A.P., Heslop, D., Zhao, X. & Pike, C.R., 2014. Understanding fine magnetic particle systems through use of first-order reversal curve diagrams. *Rev. Geophys.,* **52,** 557–602.

Roberts, A.P., Pike, C.R. & Verosub, K.L., 2000. First-order reversal curve diagrams: a new tool for characterizing the magnetic properties of natural samples. *J. geophys. Res. Solid Earth.,* **105,** 28461–28475,

Robertson, D.J. & France, D.E., 1994. Discrimination of remanence-carrying minerals in mixtures, using isothermal remanent magnetisation acquisition curves. *Phys. Earth planet. Inter.,* **82,** 223–234.

Sagnotti, L. & Winkler, A., 2012. On the magnetic characterization and quantification of the superparamagnetic fraction of traffic-related urban airborne PM in Rome, Italy. *Atmos. Environ.,* **59,** 131–140.

Sagnotti, L., Macri, P., Egli, R. & Mondino, M., 2006. Magnetic properties of atmospheric particulate matter from automatic air sampler stations in Latium (Italy): toward a definition of magnetic fingerprints for natural and anthropogenic PM 10 sources. *J. geophys. Res.,* **111,** B12S22. doi:10.1029/2006JB004508.

Sagnotti, L., Taddeucci, J., Winkler, A. & Cavallo, A., 2009. Compositional, morphological, and hysteresis characterization of magnetic airborne particulate matter in Rome, Italy. *Geochem. Geophys. Geosyst.,* **10**. doi:10.1029/2006JB004508.

Sanderson, P., Su, S.S., Chang, I.T.H., Delgado Saborit, J.M., Kepaptsoglou, D.M., Weber, R.J.M. & Harrison, R.M., 2016. Characterisation of iron-rich atmospheric submicrometre particles in the roadside environment. *Atmos. Environ.,* **140,** 167–175.

Seinfeld, J.H. & Pandis, S.N., 2016. Properties of the Atmospheric Aerosol. in: *Atmospheric Chemistry and Physics: from Air Pollution to Climate Change*. John Wiley & Sons, Hoboken, NJ, pp. 325–359.

Sheikh, H.A., Maher, B.A., Karloukovski, V., Lampronti, G.I. & Harrison, R.J., 2022. Biomagnetic characterization of air pollution particulates in Lahore, Pakistan. *Geochem. Geophys. Geosyst.,* **23**. doi:10.1029/2021GC010293.

Shu, J., Dearing, J.A., Morse, A.P., Yu, L.Z. & Li, C.Y., 2000. Magnetic properties of daily sampled total suspended particulates in Shanghai. *Environ. Sci. Technol.,* **34,** 2393–2400.

Spassov, S., Egli, R., Heller, F., Nourgaliev, D.K. & Hannam, J., 2004. Magnetic quantification of urban pollution sources in atmospheric particulate matter. *Geophys. J. Int.,* **159**(2), 555–564.

Stancu, A., Pike, C., Stoleriu, L., Postolache, P. & Cimpoesu, D., 2003. Micromagnetic and preisach analysis of the First Order Reversal curves (FORC) diagram. *J. appl. Phys.,* **93,** 6620–6622.

Stone, V. *et al.*, 2017. Nanomaterials versus ambient ultrafine particles: an opportunity to exchange toxicology knowledge. *Environ. Health Perspect.,* **125,** doi:10.1289/EHP424.

Szonyi, M., Sagnotti, L. & Hirt, A.M., 2008. A refined bio-monitoring study of airborne particulate matter pollution in Rome, with magnetic measurements on Quercus Ilex tree leaves. *Geophys. J. Int.,* **173**(1), 127–141.

Szuszkiewicz, M.M., Łukasik, A., Petrovský, E., Grison, H., Błońska, E., Lasota, J. & Szuszkiewicz, M., 2023. Magneto-chemical characterisation of Saharan dust deposited on snow in Poland. *Environ. Res.,* **216,** doi:10.1016/j.envres.2022.114605.

Thorpe, A. & Harrison, R.M., 2008. Sources and properties of non-exhaust particulate matter from road traffic: a review. *Sci. Total Environ.,* **400,** 270–282.

Vlasov, D., Ramírez, O. & Luhar, A., 2022. Road dust in urban and industrial environments: sources, pollutants, impacts, and management. *Atmosphere,* **13,** 10.3390/atmos13040607.

Winkler, A., Amoroso, A., di Giosa, A. & Marchesani, G., 2021. The effect of Covid-19 lockdown on airborne particulate matter in Rome, Italy: a magnetic point of view. *Environ. Pollut.,* **291,** doi:10.1016/j.envpol.2021.118191.

Winkler, A., Contardo, T., Lapenta, V., Sgamellotti, A. & Loppi, S., 2022. Assessing the impact of vehicular particulate matter on cultural heritage by magnetic biomonitoring at Villa Farnesina in Rome, Italy. *Sci. Total Environ.,* **823,** 153729. doi:10.1016/j.scitotenv.2022.153729.

Xie, S., Dearing, J.A., Bloemendal, J. & Boyle, J.F., 1999. Association between the organic matter content and magnetic properties in street dust, Liverpool, UK. *Sci. Total Environ.,* **241,** 205–214.

Xie, S., Dearing, J.A., Boyle, J.F., Bloemendal, J. & Morse, A.P., 2001. Association between magnetic properties and element concentrations of Liverpool street dust and its implications. *J. appl. Geophys.,* **48,** 83–92.

Yang, Y., Vance, M., Tou, F., Tiwari, A., Liu, M. & Hochella, M.F., 2016. Nanoparticles in road dust from impervious urban surfaces: distribution, identification, and environmental implications. *Environ. Sci. Nano,* **3,** 534–544.